MARCH 1982

REQ. NO. 9-9094

CONTRACT REPORT NO. OSQ80-00041

FINAL REPORT

The Preparation and Characterization of TiO_2 Thick Film Photoanodes for Applications In Photoelectrochemical Cell.

Contract #: 18SQ.23440-9-9094

PREPARED FOR: Canada Center for Mineral
and Energy Technology
555 Booth Street
Ottawa, Ont.
K1A 0G1

PREPARED BY: Bell Northern Research Ltd.
P.O. Box 3511, Station
Ottawa, Ont.
K1Y 4H7

97PP

January 1982

The Preparation and Characterization of TiO_2 Thick Film Photoanodes for Applications In Photoelectrochemical Cells.

Contract #: 18SQ.23440-9-9094

FINAL REPORT

Prepared by C. Blaauw and H.M. Naguib

Recommended: _____
W.D. Westwood, Manager, Materials and Device Research

Approved: _____
R.J. Kriegler, Manager, Advanced Technology Laboratory

Released: _____
R. Kenedi, Vice-President, Systems Division

TABLE OF CONTENTS

		Page
	SUMMARY	(i)
I.	INTRODUCTION	1
II.	BACKGROUND	4
	II.1 Photoelectrochemical Solar Cells	4
	II.2 Thick Film Technology	8
III.	EXPERIMENTAL PROCEDURES	13
	III.1 Paste Preparation	13
	III.2 Fabrication of Photoanodes	13
	III.3 Materials Characterization and Analysis	19
IV.	THE EFFECT OF GLASS COMPONENT ON THE PROPERTIES OF TiO_2 THICK FILMS	28
	IV.1 Objectives and Experimental Details	28
	IV.2 Results and Discussion	28
	IV.3 Conclusions	39
V.	FRITLESS ANATASE-BASED THICK FILMS	40
	V.1 Objectives and Experimental Details	40
	V.2 Results and Analysis	40
	V.3 Discussion	67
	V.4 Conclusions	73
VI.	COMPLEMENTARY INVESTIGATIONS	75
	VI.1 Objectives	75
	VI.2 The effect of anatase phase	75
	VI.3 The effect of dopants	77
	VI.4 Conclusions	82
VII.	OVERALL CONCLUSIONS	83
	REFERENCES	87

SUMMARY

The purpose of this work was to determine the feasibility of fabricating screen-printed thick film photoanodes and investigate their properties for use in photoelectrochemical (PEC) cells. Screen printing is a standard manufacturing technique in the electronics industry and would provide an economical method for the fabrication of PEC electrodes. TiO_2 was chosen as the electrode material because it is currently one of the most investigated semiconductor anode in PEC cells.

TiO_2 thick film pastes were prepared from rutile and/or anatase powders, mixed with varying amounts of glass frit (0-25%) and dispersed in a liquid organic vehicle. The films were screen printed on gold-metallized alumina substrates and air-fired in a belt conveyor furnace at peak temperatures in the range 600-900 °C. The as-fired photoanodes were then made conducting by heating in ammonia or hydrogen atmospheres at temperatures in the range 400-900 °C. The films were characterized by scanning electron microscopy, x-ray diffraction, x-ray fluorescence, nuclear microanalysis, elastic recoil detection, proton-induced x-ray emission, and electrical resistivity measurements. In addition, their photoelectrochemical properties were determined at the Physical Chemistry Section of the Mineral Science Laboratories, CANMET, Department of

Energy, Mines and Resources, Ottawa.

The presence of glass frit in the film provided good adhesion but reduced the active region for the absorption of light in the photoanode and decreased the electron transfer efficiency at the electrolyte/semiconductor interface. However, the use of glass was eliminated by using TiO_2 powder of the anatase structure. During firing, anatase undergoes a transformation to the rutile phase which enhances the sintering of the TiO_2 particles and provides good adhesion of these particles to the substrate. An optimum air firing cycle of 90 min at a peak temperature of 900°C was established for anatase-based thick films. The as-fired films had undergone 80% transformation to the rutile phase. The thickness, grain size and density of the films were determined to be 30 μm, 0.2 μm and 2 g/cm^3, respectively.

A number of impurities were detected in the as-fired films. These were found to originate from the initial powder (Na, K, Si, Mg and V), contamination during paste preparation (Al and Zr) and diffusion of impurity elements (e.g. Cu) from the gold-metallized substrates during the firing cycle.

The use of ammonia as a reducing agent produced films with a high concentration of oxygen vacancies and lower

oxides with metallic properties. These resulted in poor PEC characteristics and low solar conversion efficiencies. Films reduced in hydrogen at 700°C showed a minor compositional change and yielded solar energy conversion efficiencies of 2.5 - 3.0% with external bias of 240 mV and 2.2 - 2.5% without bias in 1M NaOH electrolyte at pH = 13. This is ~ 40% higher than the corresponding efficiency obtained from rutile single crystal electrodes reduced under the same conditions. Also, the hydrogen-reduced thick films exhibited larger absorption of light energy in the long wavelength region.

The improved PEC characteristics of the screen printed thick films have been attributed to a number of factors. These include the nature of the internal (porous) structure of the thick films, the existence of a high level of certain beneficial impurities, low contact resistance at the back metallization interface, a rough, light-absorbing surface with a large semiconductor/electrolyte interface area, and the presence of a residual anatase layer at the film surface.

In addition, preliminary experiments showed that the addition of Al_2O_3 improves the photocurrent response of anatase-based films and thereby their solar conversion efficiency. However, the addition of 3d transition metals decreases the conversion efficiency but increases the

wavelength response in the visible region.

In conclusion, this investigation has demonstrated the potential use of thick film technology as a practical, low cost method for the fabrication of TiO_2 photoanodes. Further investigation is required to determine the effects of the various factors responsible for the high conversion efficiency of the thick films and to allow the development of an economical PEC solar cell.

I. INTRODUCTION

The original objectives of this research contract were to:

1) prepare and characterize semiconducting TiO_2 thick film electrodes for use in photoelectrochemical (PEC) cells.

2) explore the feasibility of hydrogenated amorphous silicon (a-Si:H) thin film electrodes for applications in PEC cells.

During the first few months of the project, emphasis was placed on the preparation of screen-printable TiO_2 pastes and the establishment of optimum printing and firing conditions on alumina substrates. At the same time, a BNR-funded program had determined the optimum parameters for the plasma deposition of a-Si:H thin films. However, preliminary investigation on the PEC characteristics of the amorphous thin films indicated that this material is not promising for PEC applications. A decision was then made to concentrate our efforts on achieving the first objective, namely the fabrication and characterization of thick film TiO_2 photoanodes.

This report presents a comprehensive coverage of the work undertaken to achieve the above objective. Following this introduction, Sec. II gives a brief background on photoelectrochemical solar cells and a description of the thick film screen-printing technique. Basic experimental

procedures undertaken for paste preparation, photoanode fabrication and various analytical techniques used in the present work are described in Sec. III. Early experiments designed to determine the effect of glass binder on the properties of anatase-and rutile- based thick films are presented in Sec. IV. The results of this section showed that good adhesion of anatase-based thick films can be achieved without the use of a glass binder by taking advantage of diffusion-enhanced sintering during anatase-rutile phase transformation. Accordingly, a detailed investigation was undertaken to determine the effect of various processing parameters on the properties of fritless anatase-based thick films. Of particular interest was the effect of post-firing reduction cycles in ammonia and hydrogen atmospheres. The results of this study on fritless anatase-based thick films are presented and discussed in Sec. V. A preliminary investigation was also carried out to determine the effect of the presence of anatase phase and the addition of extraneous impurities on the PEC properties of the thick films. This work is discussed in Sec. VI. Finally, the overall conclusions, recommendations and suggestions for future work are outlined in Sec. VII.

It should be pointed out that the work described in this report regarding the preparation of TiO_2 thick films, the fabrication of photoanodes and the evaluation of their

compositional, structural, physical and electrical properties was undertaken at BNR's Advanced Technology Laboratory. The photoelectrochemical studies were carried out at the Physical Chemistry Section of the Mineral Science Laboratories, CANMET, Department of Energy, Mines and Resource, Ottawa, by A. Ahmed , G. Davidson and S.M. Ahmed . These studies consisted of voltametric measurements on BNR's TiO_2 anodes in the dark, measurements of photocurrents, spectral response and estimations of the solar conversion efficiency of the PEC cells. The results of the CANMET-EMR's group were submitted to BNR and are included in this report in agreement with the terms of the R and D contract.

II. BACKGROUND

II.1 Photoelectrochemical Solar Cells

In its simplest form, a photoelectrochemical cell (PEC) consists of two electrodes immersed in an aqueous electrolyte and connected electrically by a wire, as shown in Fig. 1. One of these electrodes is a metal that does not react chemically with the electrolyte; the other electrode is a semiconductor with one face in contact with the electrolyte and the other face connected to the shorting wire by an ohmic contact. Ideally, when light falls on the semiconductor electrode, oxygen gas is liberated at one electrode and hydrogen is liberated at the other.

Recently, a number of review articles have been published on hydrogen generation in PEC cells (1-6). The operation of such a cell can be generally explained in terms of electron energy levels in the electrodes and the electrolyte. For an n-type semiconductor photoanode, light incident upon the semiconductor with energy $h\nu$ greater than the energy gap of the material, E_g, results in the generation of an electron-hole pair. This pair is separated by the electric field in the depletion region. Under the influence of this electric field the electrons move away from the surface into the bulk of the semiconductor and then transfer via the external circuit to the metal counter-electrode where they discharge H_2 according to the

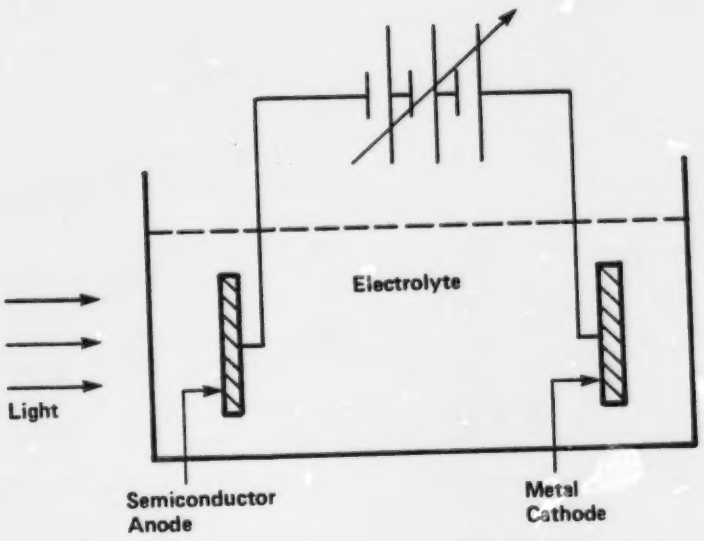

(a)

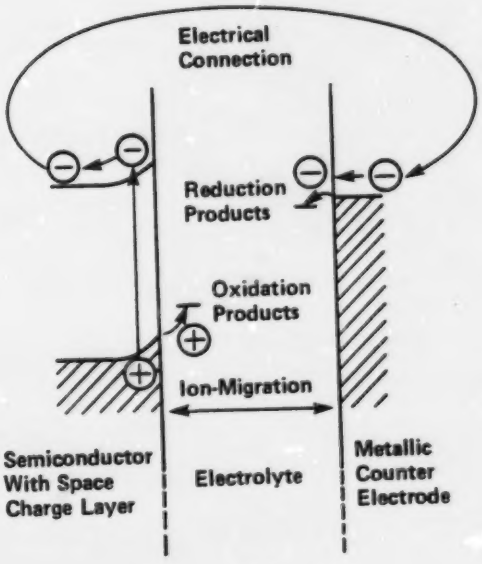

(b)

Fig. (1) (a) A schematic representation of a PEC cell and (b) the principle of its operation.

reaction:

$$2H^+ + 2e^- \longrightarrow H_2 \uparrow \quad \text{(cathode)}$$

The holes, on the other hand, move in the depletion region's electric field to the semiconductor-electrolyte interface and oxidize water molecules in the solution to discharge O_2 according to the reaction:

$$H_2O + 2p \longrightarrow \tfrac{1}{2}\, O_2 \uparrow + 2H^+ \quad \text{(Photoanode)}$$

For p-type semiconducting photoanodes a hole depletion region is formed with the photogenerated electrons moving to the semiconductor/electrolyte interface and the holes transferred via the external circuit to the metal counter-electrode (anode). Accordingly, hydrogen is liberated at the semiconductor electrode and oxygen at the metal counter-electrode.

The basic characteristics for a semiconductor material to be used effectively in PEC cells are the following (4,5):

1. Appropriate work function and flat band potential to produce sufficient band bending to prevent hole-electron recombination at the electrolyte-semiconductor interface.

2. A band gap somewhat greater than the energy required to decompose water (1.23 eV) plus an allowance for band bending, overvoltage and resistance of the semiconductor and

the electrolyte, but small enough to absorb an appreciable portion of the solar spectrum.

3. Appropriate bulk and surface properties for efficient tunneling and band bending to eliminate the need for extra bias.

4. Electrochemical stability against corrosion, so that the water decomposition reaction predominates over the electrode decomposition reaction.

TiO_2 is one of the most commonly used anode material in PEC systems. Unfortunately, the work function of TiO_2 is such that an external bias of about 0.3V is required to produce hydrogen in the PEC cells. Furthermore, its optical band gap of 3 eV corresponds to an absorption edge of about 400 nm, too far into the U.V. region to significantly absorb solar energy. A great amount of work has been done to find the right semiconductor that satisfies the requirements for PEC applications (1-6). In general, for a given class of materials, as the band gap decreases the electron affinity increases and the chemical stability of the materials degrades(6). Accordingly, among over two dozen semiconductor materials investigated to date, TiO_2 remains high in the list of materials suitable for PEC cells because of its high electrochemical stability.

TiO_2 based photoanodes have been fabricated using single crystals (e.g. 7) and polycrystalline films prepared by a variety of techniques including chemical vapor deposition (e.g. 8,9), thermal oxidation (e.g. 10,11) or anodic oxidation of thin Ti foils (e.g. 12, 13), hot pressing of TiO_2 powder (e.g. 13), plasma spraying (e.g. 14,15), and reactive sputtering (16). Although TiO_2 thick films are used as dielectric materials in the fabrication of microelectronic products (17,18), the adaptation of such films for PEC applications has not been reported in the literature. Before going into the experimental details designed to achieve this goal, a brief description of the thick film processing technique is presented in the following section.

II.2 Thick Film Technology

In the field of microelectronics, thick film technology is referred to as the process by which passive microcircuit components are formed by screen printing of specially formulated pastes on ceramic substrates, followed by firing at high temperatures to sinter the materials to the substrate (19). Typically, the thickness of a thick film element is 12-25 μm. This distinguishes it from thin film technology where the materials are deposited by chemical or physical vapour deposition or by sputtering techniques to thicknesses up to 1 μm (20). The thin film passive

components are registered on the substrate using masks in the deposition system or by applying standard photolithographic techniques.

Thick film pastes usually consist of three components: an organic vehicle, glass frit and active materials. The active materials may be elemental metals or alloys for conductor films, semiconducting compounds or alloys for resistor films or dielectric materials for insulating layers. The glass frit serves as a bonding agent between the active particles and provides adhesion of the films to the substrate. Some pastes do not contain glass frit and are referred to as "molecular bonding" or "fritless" pastes. The organic vehicle provides the flow characteristics of the paste. A typical organic vehicle consists of a mixture of ethyl-cellulose, butyl-carbitol acetate and an organic solvent such as isopentyl solicylate or β-terpinol.

The thick film composition is generally applied to the substrate by screen printing. Dipping, brushing or spraying are occasionally used with irregularly shaped substrates. The screen printing process consists of forcing the thick film compositions through a stainless steel woven mesh screen onto the substrate with a squeegee. An open pattern in the screen defines the structure which will be printed on the substrate. The printing process takes place in a "screen printer" which is a precision apparatus that

provides means for mounting the screen, positioning the screen relative to the substrate in x, y, z and angle, positioning the squeegee relative to the screen and moving the squeegee with a controlled speed and pressure. In a typical screen printing process the screen is positioned at a precise distance above the substrate (500-1000 μm). This distance is called the "snap-off distance". The ink is spread on the screen by a spreading bar, while the squeegee is in a retracted position. The squeegee is then applied to the screen with a controlled pressure and speed to maintain a constant angle of attack during the printing stroke. As the squeegee passes, it brings the screen into contact with the substrate, transferring the ink to the substrate in the desired pattern. The process steps are shown in Fig. 2.

After printing the film is dried in an infrared belt conveyor furnace for a period of 10-15 min at a typical peak temperature of 150°C. During the drying cycle, the volatile organic solvents evaporate leaving a dry film held to the substrate by the remaining polymeric part of the vehicle. The dried film is then fired in a belt conveyor furnace with four or more resistance heated zones. A time-temperature profile during a typical thick film firing cycle is shown in Fig. 3. During the initial portion of the firing process, the film is gradually heated (typically 30 - 70 °C/min) through the temperature range from 200 to 450°C. During this period the remaining organic materials are volatilized

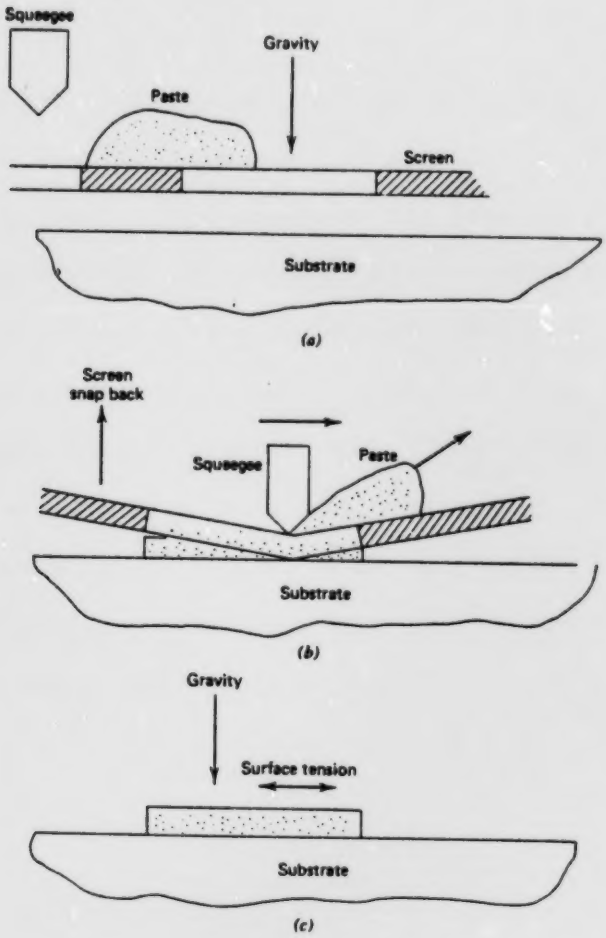

Fig. (2) The screen printing thick film process.

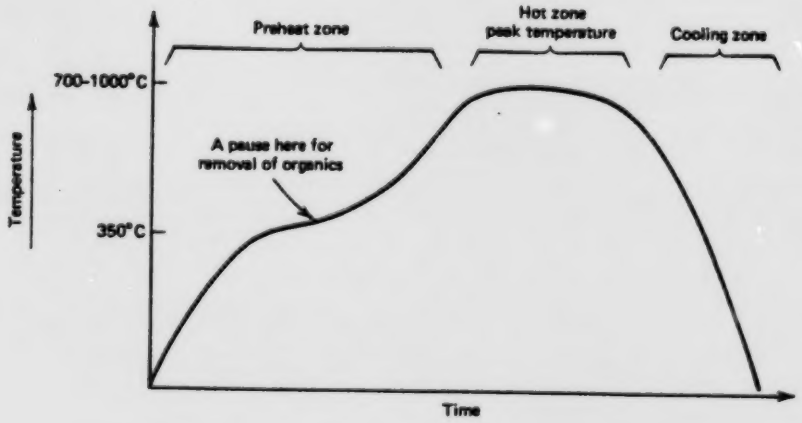

Fig. (3) Typical firing profile for thick film materials.

and burned-off. To ensure the complete removal of all organics, sufficient time and good ventilation with clean air are required. Depending upon the type of ink being fired, various events occur above 450°C including glass flow and chemical reactions. Holding the substrate at peak temperature (generally 10 min at 850°C for films fired on alumina substrates) ensures that these changes occur reproducibly. The film must then be gradually cooled at a typical rate of 30 - 70°C/min to anneal the film and relief stresses. After firing, the film becomes part of the ceramic substrate with the organic vehicle entirely removed.

III. EXPERIMENTAL PROCEDURES

III.1 Paste Preparation

All pastes were prepared from TiO_2 powder purchased from Baker Chemical Co. having both the rutile and the anatase structures. The major impurities in these powders as determined by x-ray fluorescence analysis are summarized in table I. Glass frit was used as a binder in the preparation of some pastes. Corning borosilicate glass #7054 was chosen because of its thermal expansion coefficient compatibility with 96% alumina substrates.

As a general procedure, powders were first ground for several hours in an alumina milling jar using zirconia grinding pellets. Freon TF was used as a wet grinding medium. After drying, the powders were passed through a 400 mesh sieve to remove any agglomerate larger than 40 μm. The powders were then combined with a liquid organic vehicle to form a paste with 50% solids. Ferro's Co-8 thick film organic vehicle was used in the preparation of all pastes. The paste viscosity was adjusted to approximately 350 poise to provide suitable screen printing conditions.

III.2 Fabrication of Photoanodes

A schematic diagram of a TiO_2 thick film photoanode is shown in Fig. 4. It consists of a TiO_2 thick film layer

TABLE 1

Chemical analysis of TiO_2 powders

used for thick film paste preparation (ppm).

Element	Anatase[1]	Rutile[2]
Si	10^3	30
Al	5×10^2	<1
Fe	2×10^2	50
Mg	10^2	5
Ca	----	2
Na	10^2	<1
K	5×10^2	---
Cl	----	<5
V	5×10^3	7
Cr	----	10
Ni	----	2
Cu	----	2
Zr	50	---
Nb	10^2	---
Ba	50	---
Zn	10	---
Pb	2×10^2	1

(1) Baker Reagent grade. Semi-quantitative x-ray fluorescence analysis carried out by Bondar-Clegg & Co. Ltd. Only quantities in excess of 30 ppm are listed.

(2) Baker Ultrex. Lot analysis as supplied by the manufacturer.

screen printed and fired on an alumina ceramic substrate. A layer of screen printed thick film conductor is also included to provide a conducting path to the counter electrode in the PEC cell. The area of the photoanodes fabricated in the present work was ~ 1 cm^2. This size was chosen to be suitable for PEC measurements. However, screen printing thick film technology has been applied to ceramic substrates as large as 22.9 cm x 7.6 cm (21) whereas 10 cm x 10 cm alumina substrates are being used routinely in the electronic industry. The preparation of large area thick film photoanodes is therefore possible.

A test pattern was designed to provide a set of eight photoanodes on each 5.1 cm x 5.1 cm alumina substrate. Three additional structures were also included in the test pattern to allow for material characterization such as electrical measurements and x-ray and ion beam analyses. The photomasks for the metallization and the TiO_2 layers in this test pattern are shown in Fig. 5.

The thick film screen printing was carried out using a deHaart AOL-12 printer. Stainless steel (st. st.) screens were used with "Micro-Film" indirect emulsion supplied by Buckbee Mears (Hudson, New Hampshire). Typical screen printing parameters used were: a squeegee pressure of 20-30 psi, a squeegee speed of 2.5 cm/s and a snap-off distance of ~ 1 mm. A Tempress-Lindberg multi-atmosphere (Air, N_2

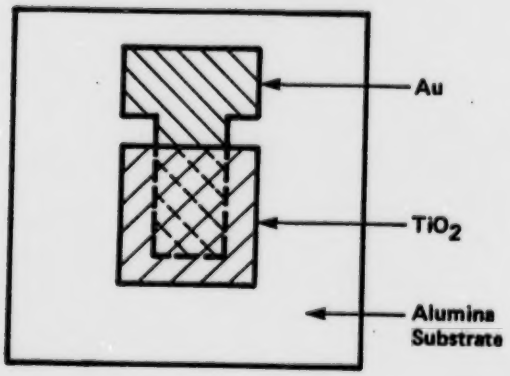

Fig. (4) A schematic diagram of a TiO_2 thick film photoanode.

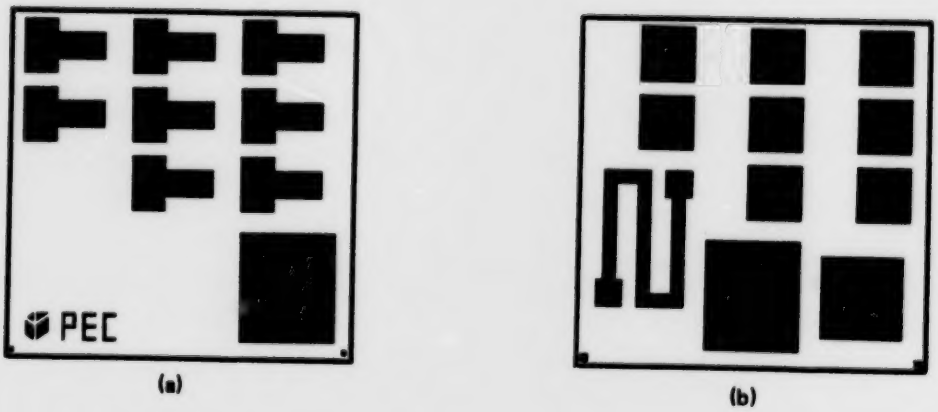

Fig. (5) Photomasks used in the preparation of thick film photoanodes (a) thick film conductor (b) TiO_2 layer.

and H_2) belt conveyor furnace was used for the drying and firing of the thick films.

The processing sequence for fabricating the thick film photoanodes can be described as follows:

1. Standard thick film 96% alumina substrates (AlSiMag #614, supplied by 3M) were ultrasonically cleaned in Freon solvents followed by firing at high temperature, typically 900°C. The use of contaminated substrates may result in poor film adhesion.

2. A layer of thick film conductor was screen printed, dried and fired as recommended by its manufacturer. In our work, we used Du Pont 9791 gold thick film ink. It was printed using a 325 screen st. st. screen, dried at 150°C for 15 min and then fired in the belt conveyor furnace using a 90 min firing cycle with 10-15 min at peak temperature of 925°C. The fired conductor had a typical thickness of 16-19 μm and a sheet resistivity of 2.3 mΩ/□.

3. A layer of TiO_2 thick film was screen printed through a 200 mesh st. st. screen to overlap the as-fired conductor electrodes, as shown in Fig. 4. The films were fired in the belt conveyor furnace with a 90 min cycle in air which included a 15 min soaking period at a peak temperature of 850-900°C.

4. A second layer of TiO_2 was screen printed and fired following the same procedure described above. As will be discussed in subsequent sections, the addition of this layer is essential to eliminate pinholes in the as-fired films. The final thickness of the TiO_2 thick film after firing the second layer was ~ 30 μm. A few samples were prepared using 3 or 4 layers of TiO_2 film for PEC characterization.

5. The as-fired TiO_2 thick film photoanodes were subjected to a thermal heating cycle in a reducing atmosphere to optimize their electrical and PEC properties. Most reduction experiments were carried out in a tube furnace using NH_3 or a mixture of Ar-20% H_2 for a period of one hour at temperatures in the range 400-900°C. The samples were first stabilized at the desired temperature in an inert atmosphere (N_2 or Ar). The reducing gas was then admitted into the tube furnace at a rate of 2000 sccm. Upon completion of the reduction cycle, the furnace was flushed with N_2 or Ar gas and allowed to cool down to ~ 300°C before removing the samples. A few reduction experiments were carried out in a H_2 atmosphere in the belt conveyor furnace. A 30 min cycle was used at peak temperatures in the range 500-900°C. This method of reduction allows a high throughput of samples under reproducible conditions and would be most attractive for commercial applications.

6. Following the reduction heat treatment step, the fabrication of each photoanode is completed by attaching a Cu wire to the thick film conductor layer by soldering or by applying silver epoxy. Fig. 6 is a photograph of a completely fabricated TiO_2 thick film photoanode.

III.3 Materials Characterization and Analysis

This section describes the analytical techniques used to investigate the effect of various processing parameters on the properties of TiO_2 thick film photoanodes.

III.3.1 X-ray Diffraction

The crystal structure of TiO_2 samples was determined at BNR by x-ray diffracion using a Philips diffractometer and CuK_α radiation. The TiO_2 phases were identified on the basis of x-ray diffraction data published in the ASTM powder diffraction index. The degree of anatase-rutile transformation in fired samples was determined using the following formula (22), assuming no preferred orientation in the film,

$$F_R = \left(1 - \frac{1}{1 + 1.26\,\frac{I_R}{I_A}}\right) 100$$

where

F_R is the weight percentage of rutile

I_R is the most intense x-ray peak of rutile ($2\theta = 27.46°$, Cu K_α)

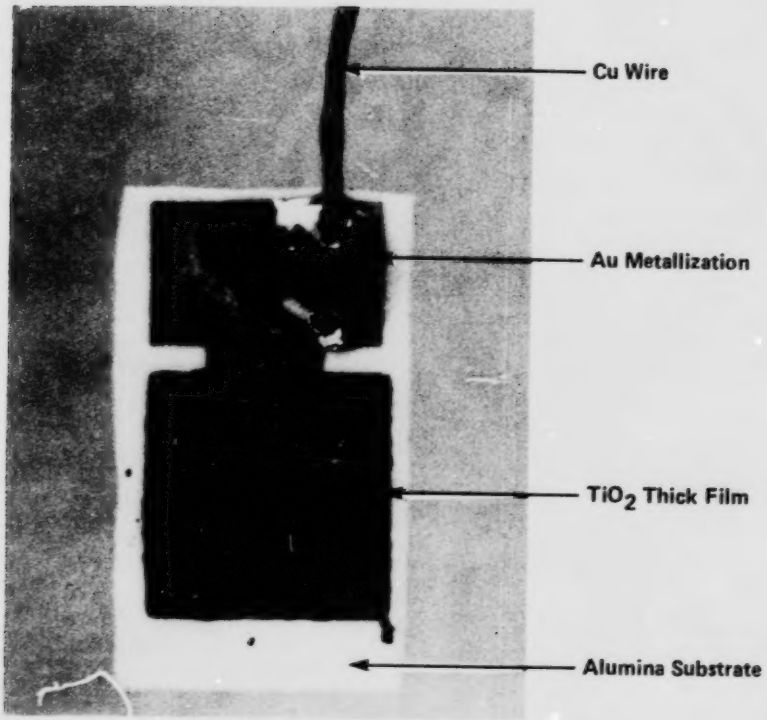

Fig. (6) Fully fabricated TiO_2 thick film photoanode.

and

I_A is the most intense x-ray peak of anatase
(2θ + 25.35°, Cu K_α)

III.3.2 Scanning Electron Microscopy (SEM)

The morphology and grain size of various samples were evaluated by SEM. This was carried out at BNR using a Jeol SEM model JSM-35-C operating at 23 KeV. The energy dispersive x-ray analyzer in the SEM was used to identify different phase agglomerates in the thick films.

III.3.3 Ion Beam Analyses

The degree of reduction and the amount of extraneous elements incorporated into the TiO_2 films during processing were determined using ion-beam analyses techniques. The analyses were conducted using a 4 MeV Van der Graaff accelerator at the nuclear physics laboratory of Queen's University.

Oxygen and nitrogen were analyzed by deuteron-induced nuclear reactions (23). To this end, films reduced under

different conditions were bombarded with 2 MeV deuterons at a typical current density of 50 nA/cm^2. Oxygen was detected using $^{16}O(d,p)^{17}O$ reaction while $^{14}N(d,\alpha)^{12}C$ and $^{14}N(d,p)^{15}N$ reactions were used to evaluate the nitrogen content. The protons and α-particles emitted were detected at an angle of 150° with a solid state detector and a multi-channel analyzer system. Corrections were made for cross-sections of the different reactions and for changes in cross-sections with increasing depth (i.e. lower energy) in the TiO_2 samples. Finally, the amounts of oxygen and nitrogen in each reduced film were determined by comparison with standard stoichiometric films of TiO_2 and TaN, respectively.

The hydrogen content was analyzed using the Elastic Recoil Detection (ERD) technique (24). A beam of 2.4 MeV α-particles was used to elastically scatter hydrogen off the target surface. The scattered particles were detected in a surface-barrier detector with a 12 μm Al foil to filter out the α-particles. Entrance and exit angles were 15° and 5° relative to the target surface. Recoil events from reduced TiO_2 samples were compared to Ti-containing H_2 standards obtained from the National Bureau of Standards, Washington, D.C.

Elements of high atomic number were analyzed by means of Proton-Induced X-Ray Emission (PIXE). This was achieved at Queen's University using a scanning proton microprobe

system that permits a high energy proton beam of 20 μm in diameter to be used in an atmospheric environment (25). The proton induced x-rays are characteristic of the elements present in the sample. Calculations have shown that the background continuum radiation produced by the PIXE technique is about three orders of magnitude lower than can be obtained from more conventional methods of x-ray excitation such as electron bombardment (26). Accordingly, the minimum detection limits for PIXE analysis are about 0.1 to 1.0 ppm. The accuracy of PIXE data has been claimed to be of the order of 5% (27) although in practice 10% has been found to be typical.

III.3.4 Electrical Resistivity Measurements

Preliminary electrical resistivity measurements were carried out on TiO_2 layers printed on alumina substrates using the standard four point probe technique. However, these films were found to be structurally different from films printed on gold metallized substrates. Therefore, further measurements were made on the photoanode samples to determine the resistance between a solder (90% In-10% Ag) dot deposited on the TiO_2 film and the gold back-metallization.

III.3.5 Photoelectrochemical Measurements

For investigating the PEC performance of the thick film TiO_2 electrodes, a copper wire was attached to the metallic backing layer of the electrode by soldering or by means of a conducting silver epoxy. The metallic backing layer, the copper wire and a portion of the TiO_2 film were then masked using silicone epoxy rubber leaving about 0.10 - 0.25 cm^2 area of the film for contact with the electrolyte in the PEC cell. The electrode was then supported by a glass tube and fitted into a Quick-Fit ground glass joint (size 14/40) with a sealed and threaded vinyl cap. The TiO_2 electrode assembly was then fitted into a multiple neck-Metrohm flask along with a Pt counter-electrode and a saturated Calomel reference electrode (SCE) to constitute an electrochemical cell. The solution used in the PEC measurements was 0.1M $LiClO_4$ at pH = 11. High purity N_2 was first bubbled through the electrolyte solutions to remove dissolved air. A simple flow of N_2 was then maintained during the PEC experiments.

Rutile single crystal electrodes were also used for comparative studies. Single crystal boules, 15-25 mm in diameter, were obtained from Commercial Crystal Laboratories, Inc. Slices 1 mm thick were sawn from these boules, using a diamond-impregnated blade, exposing the (001) surfaces. The slices were reduced in H_2 or NH_3 under conditions determined by the requirements of the comparative investigation. One side of the TiO_2 slice was then mechanically polished to a smooth shiny finish using 0.05 μm

alumina powder in the final polishing stage. Electrode assemblies were finally prepared as described above for the thick film samples.

Samples were illuminated through a quartz window in the PEC cell with a 150 W Xe-lamp provided with a suitable optical system for light collimation and focusing. The light intensity was measured using a calibrated Optometer (model 40X) supplied by United Detector Tech., (Santa Monica, Ca.). Where necessary, the light intensity was varied using neutral density filters supplied by Melles Griot Co. (Irvine, Ca.).

Electrochemical and photocurrent measurements were performed using the experimental set up shown in Fig. 7. A Wenking potentiostat, a voltage scan generator (VSG72) and a Hewlett-Packard X-Y recorder (model 7004B) were used in these experiments. Photocurrent spectra were obtained as a function of wavelength of the incident light and applied voltage (SCE) under potentiostatic conditions. A Jarrel-Ash Model 82-4TO monochromator was used for this purpose. For comparison, all spectra were recorded under the same experimental conditions to avoid errors due to light intensity variations. The photocurrent spectra reported in this work were not corrected for the spectral response of the Xe-lamp. Also, to compare the photoconversion efficiency of different samples, photocurrents for all

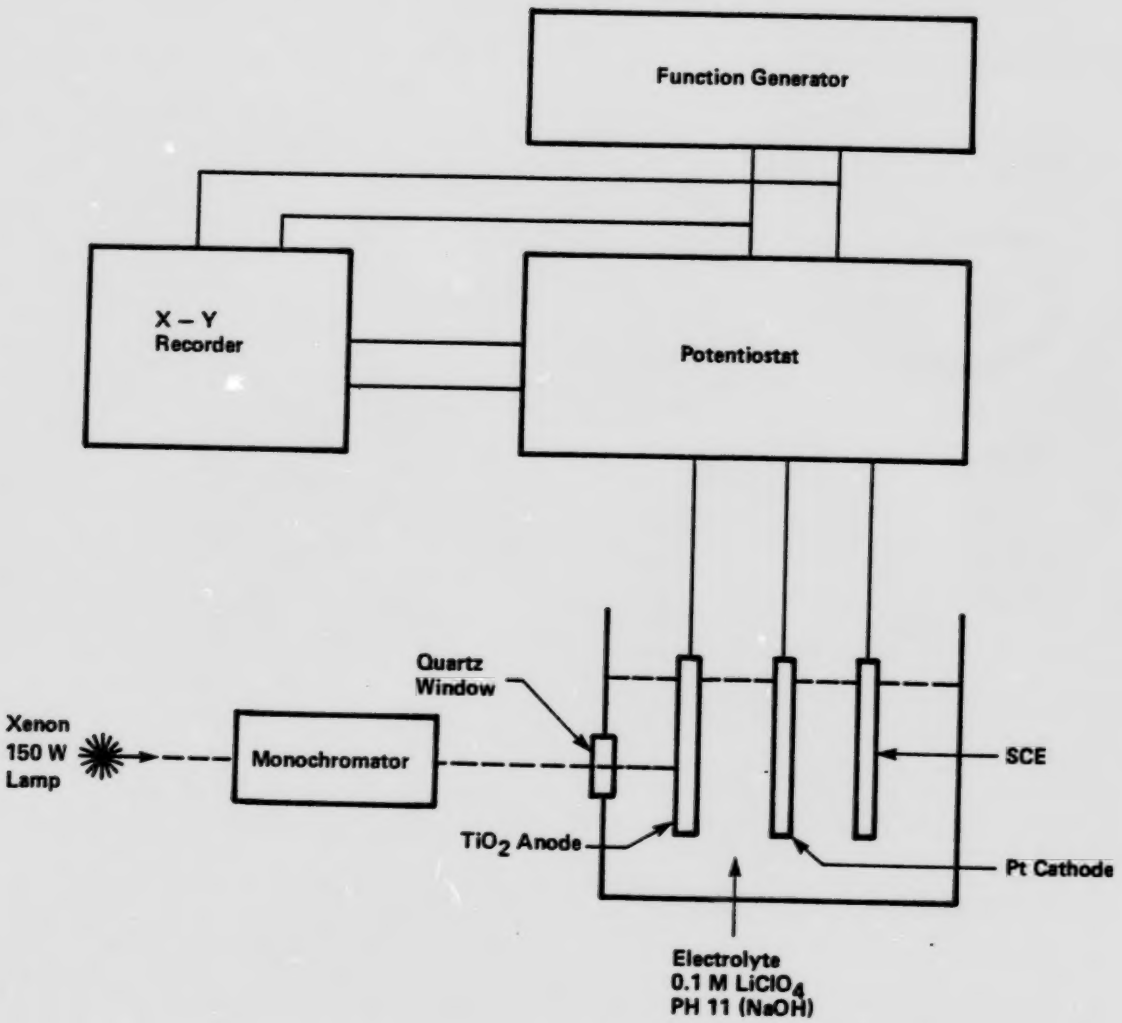

Fig. (7) Experimental set-up used for photoelectrochemical measurements of TiO_2 photoanodes.

samples were measured at an applied potential of 650 mV (SCE).

In experiments designed to determine the solar conversion efficiency, η, of the TiO_2 photoanodes, 1M NaOH was used at pH= 13. The efficiency, η, was calculated from short circuit currents, i_{sc}, (photocurrent at the reversible potential, E_R) obtained from the photocurrent spectra i_{ph} vs. voltage plots obtained under potentiostatic conditions. In some cases, a bias of 240 mV was applied over and above E_R and this bias was included in the calculation of η.

The efficiency was also determined by direct measurements of short circuit photocurrents under non-potentiostatic conditions. This is determined by measuring the voltage drop across a 100Ω resistance in series with the cell. Open circuit potentials (V_b) were measured separately against a saturated Calomel electrode. η was then calculated from the following equation:

$$\eta = i_{sc} (1.48 - V_b) \frac{100}{P}$$

where P is the power of the incident light measured in mW/cm^2.

IV. THE EFFECT OF GLASS COMPONENT ON THE PROPERTIES OF TiO_2 THICK FILMS

IV.1 Objectives and Experimental Details

The first series of experiments were carried out to determine the optimum content of glass binder to be used in TiO_2 thick films. Pastes were prepared from rutile and anatase powders mixed with varying amounts of glass binder (0-25%). The films were printed on alumina substrates, both with and without a Au-metallization layer and fired at a peak firing temperature of 850°C unless otherwise specified. Photoanodes were fabricated with 1-4 layers of TiO_2 film with each layer printed and fired separately. The samples were reduced in NH_3 atmosphere. The reduction temperatures and times were chosen to obtain a film resistivity in the order of 10 Ω. cm. These were determined to be 2 hr at 700°C for anatase-based films and 20 hr at 750°C for rutile-based films.

IV.2 Results and Discussion

IV.2.1 Adhesion and Morphology

All films showed good adhesion to the alumina substrates except those made from rutile pastes containing no glass. The good adhesion exhibited by anatase films without a glass binder has been attributed to a mechanism of phase transformation enhanced sintering. During firing at

temperatures greater than 600°C anatase transforms into rutile (28). The diffusion process associated with this transition contributes to the sintering and good adhesion of the film to the substrate. This phenomenon of phase transformation enhanced reactivitiy of solids is known as the "Hedvall Effect "(29). The transformation was confirmed by x-ray analysis as shown in Fig. 8. Furthermore, the degree of transformation, and thereby the adhesion of the film, was found to increase with increasing firing temperature and time and by reducing the particle size of the anatase powder, as shown in Figs. 9 and 10, respectively. In these results, the fraction of the anatase phase transformed into rutile was determined from the x-ray diffraction data, as described in Sec. III.3.1.

The as-fired films were also investigated by scanning electron microscopy (SEM). Typical SEM micrographs for rutile-and anatase-based films are shown in Figs. 11 and 12, respectively. The micrographs show that the glass is not uniformly distributed in the films, but forms continuous structures that completely engulf the TiO_2 particles in some areas but is totally absent in other areas of the films. A distinct difference is also observed in the morphology of anatase and rutile films. Whereas anatase films show a uniform distribution of fine grained material, rutile films contain both fine and course particles with dimensions of several microns. Also voids are prominent in the rutile

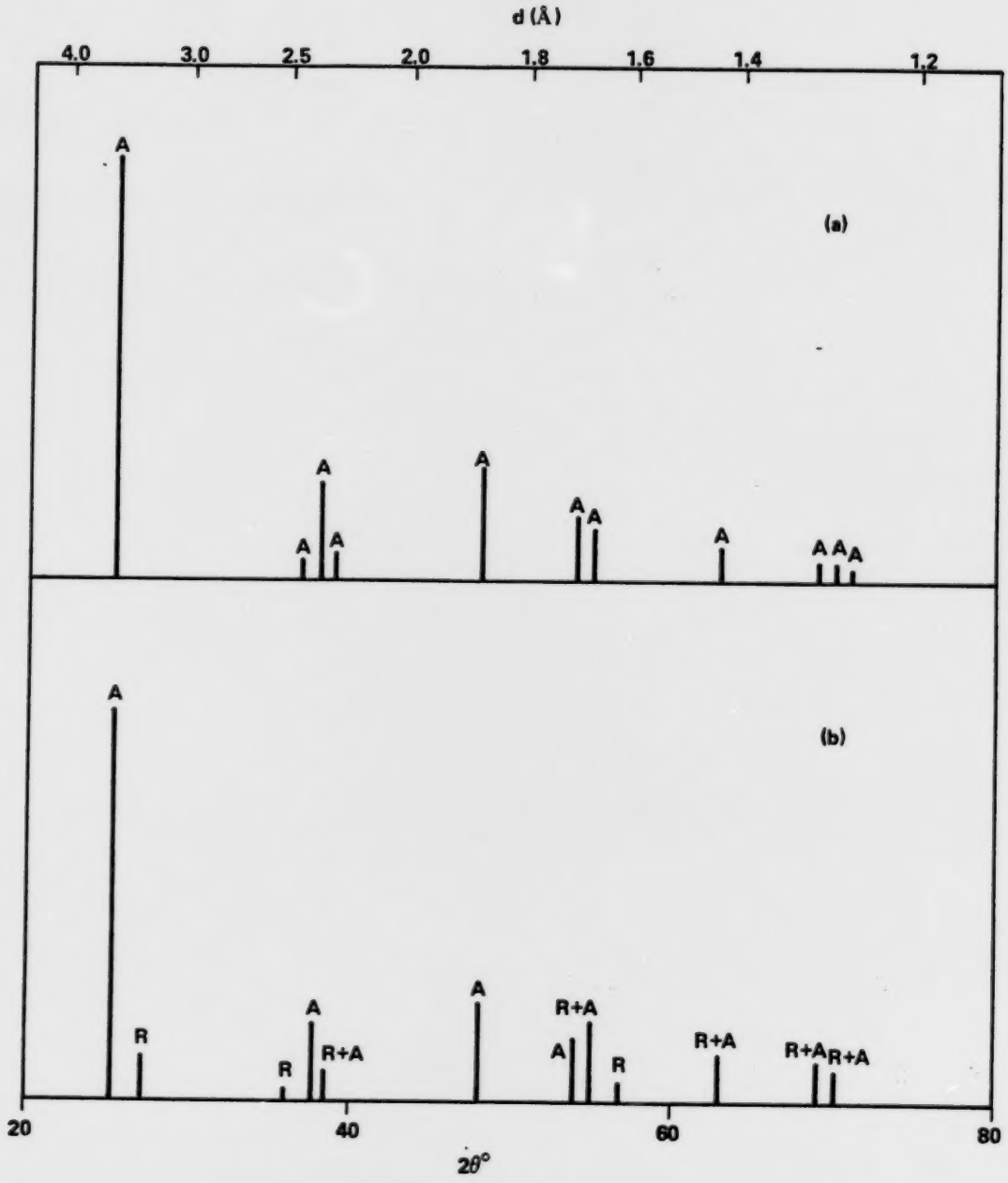

Fig. (8) X-ray spectra of anatase-based thick films printed directly on an alumina substrate a) before firing, b) after firing in air at 900°C. A and R refer to anatase and rutile, respectively.

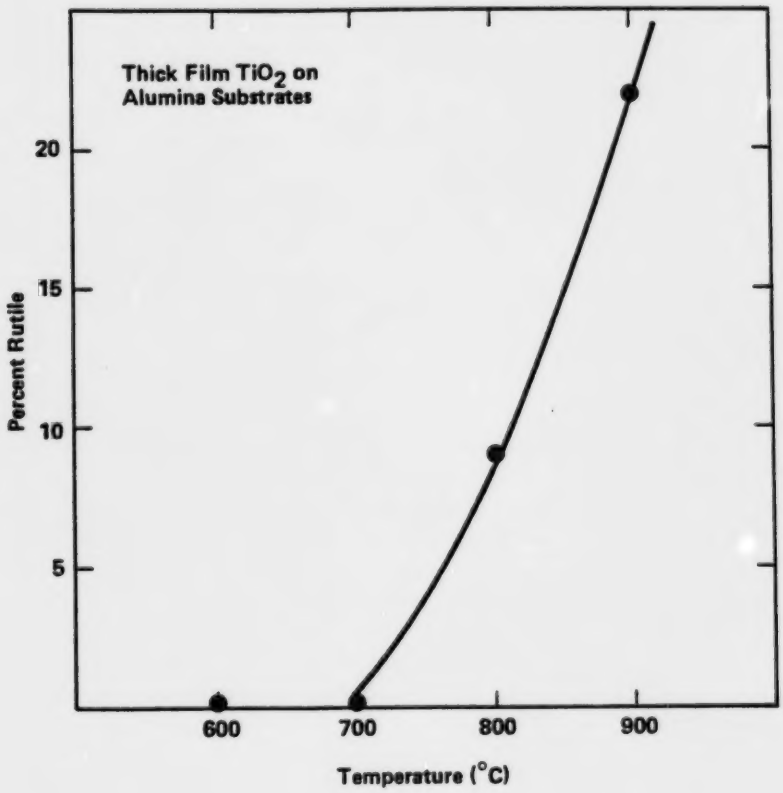

Fig. (9) Percentage of rutile phase in anatase-based thick film fired at various temperatures.

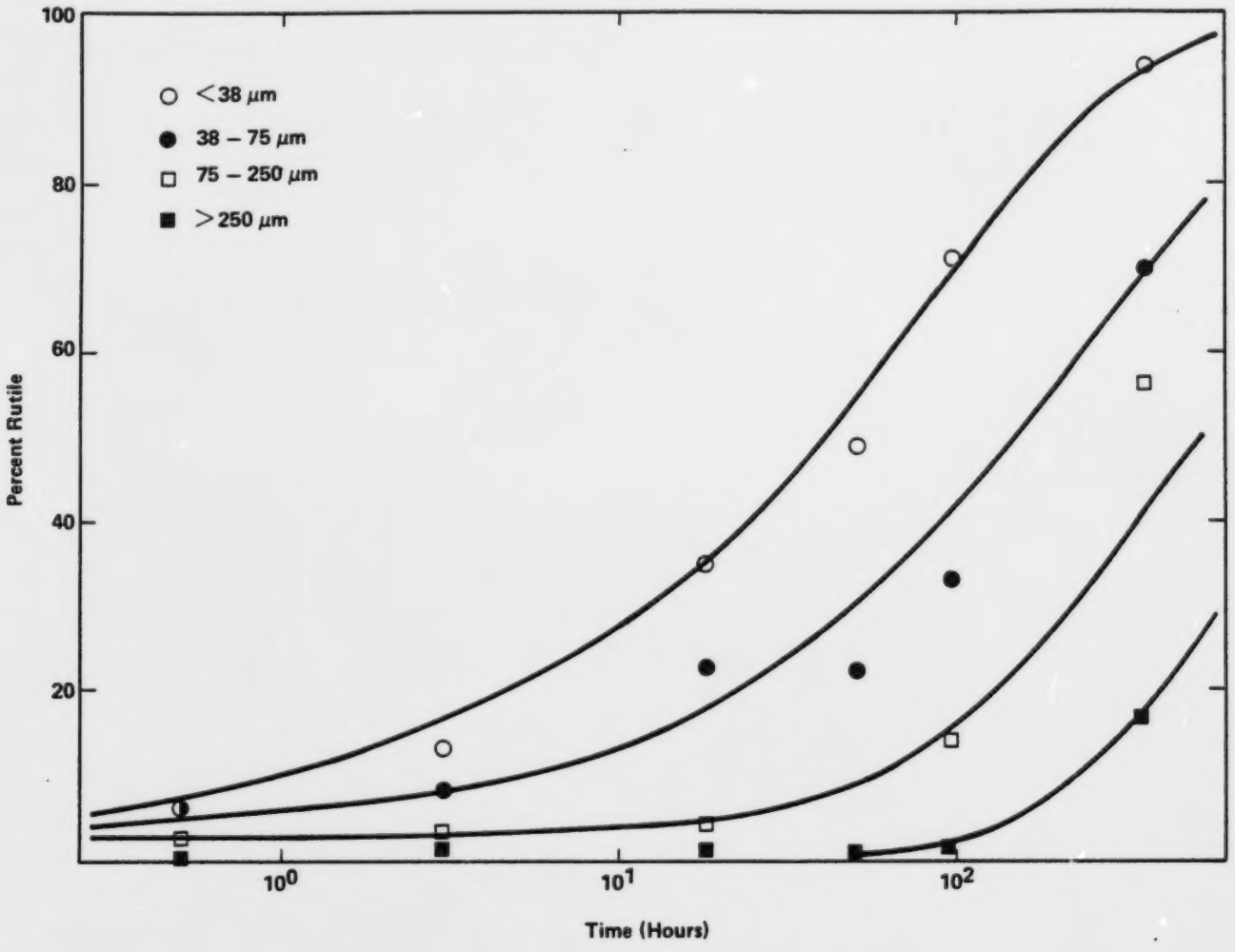

Fig. (10) Percentage of rutile phase in anatase-based thick films isothermally annealed in air at 850°C for various lengths of time. Note the effect of initial particle size of the anatase powder on the rate of anatase-rutile phase transformation.

(a)

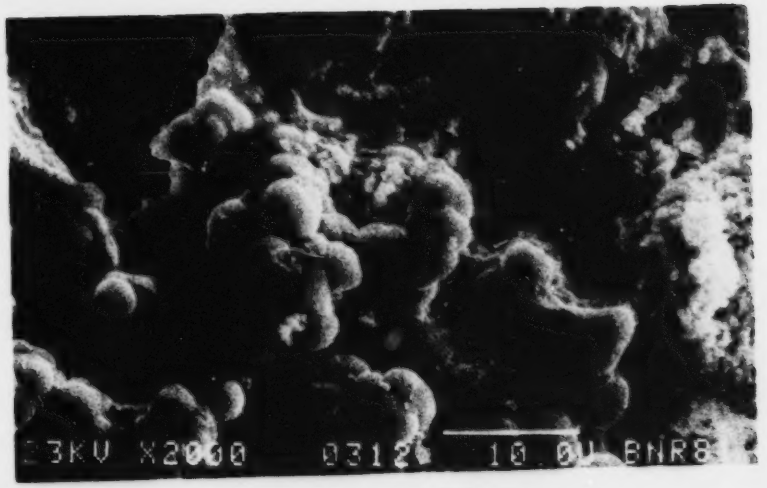

(b)

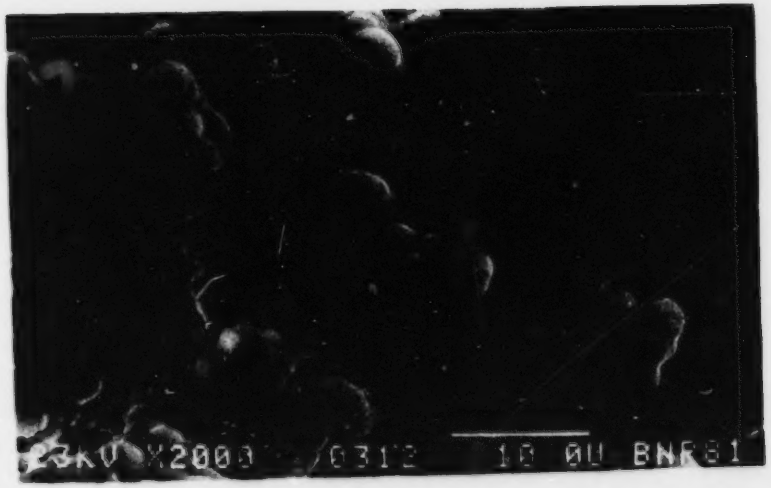

(c)

Figure 11. SEM micrographs of rutile-based thick films fired at 850°C. (a) no glass (b) 15% glass (c) 25% glass.

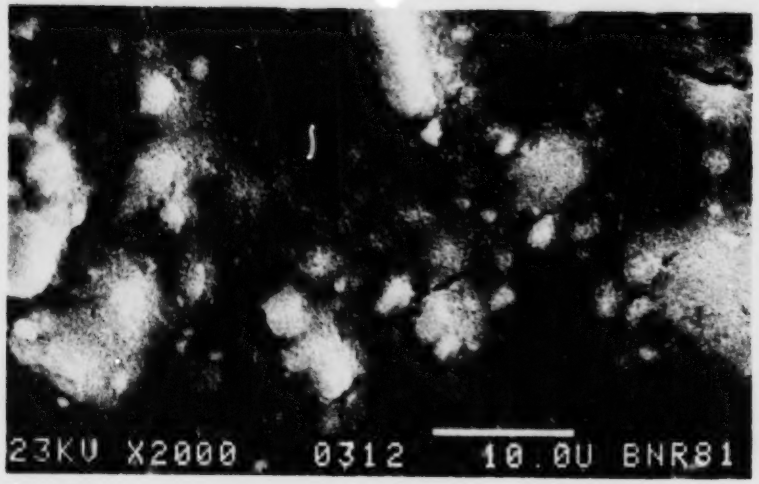

(a)

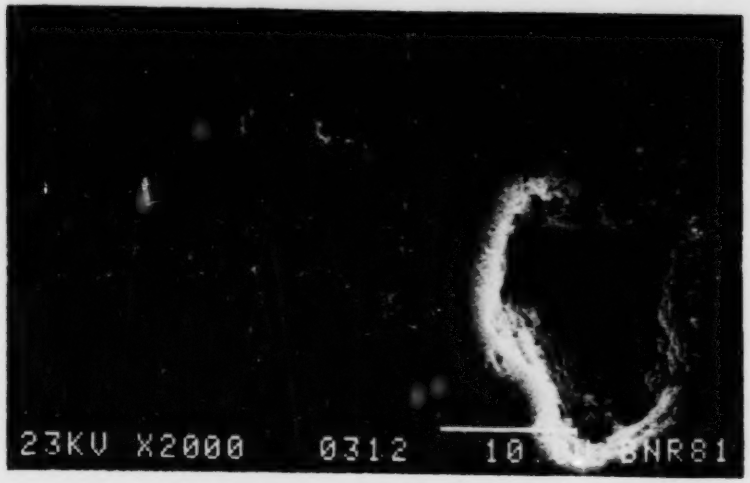

(b)

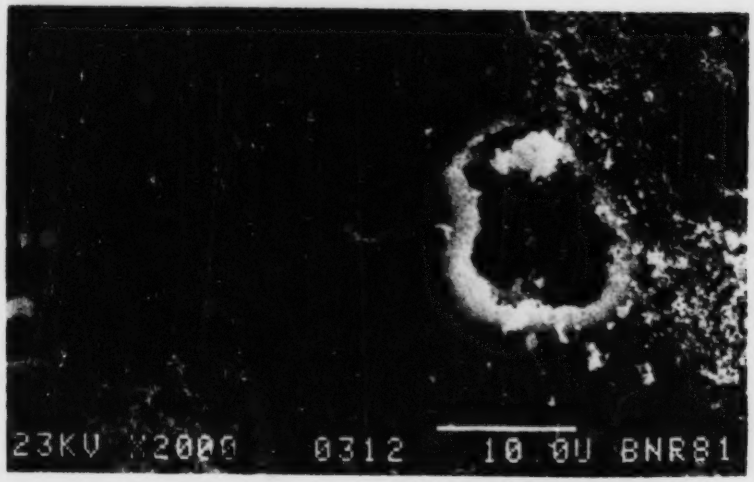

(c)

Figure 12. SEM micrographs of anatase-based thick films fired at 850°C. (a) no glass (b) 15% glass (c) 25% glass.

films. The difference in grain size distribution is thought to be caused by the different response of anatase and rutile to the grinding mechanism during the paste preparation process. Rutile and anatase have hardness constants of appoximately 6.2 and 5.7 respectively on the Mohs' scale (30) and therefore are expected to respond differently to a specific grinding procedure.

IV.2.2 PEC Characteristics

Table II summarizes typical PEC results obtained from anatase and rutile-based thick films containing various amounts of glass binder. Due to the poor adhesion of the rutile based films with no glass component, they were not included in the analysis.

In general, the films exhibited low photocurrents, large dark currents and hysteresis as compared to single crystal TiO_2. An example of a typical current-potential characteristic of a rutile-based film with 15% glass is shown in Fig.13. In some cases, the photocurrents of the thick films were one order of magnitude lower than those of single crystals reduced under the same conditions. However, there was no correlation with the amount of glass in the films.

Films consisting of one printed layer sometimes

TABLE II

Resistivity and photocurrent of anatase-and rutile-based thick film anodes, with varying amounts of glass, and a rutile single crystal anode after reduction in NH_3.

Materials	% glass	reduction conditions time(hr)	temp.(°C)	resistivity (Ω cm)	photocurrent (mA/cm^2)	comments
Anatase-based thick film	0	2	750	10	0.16	small hysteresis small dark current
	15	2	750	10	0.06	moderate hysteresis moderate dark current
	25	2	750	10	0.13	large hysteresis large dark current
Rutile-based thick film	15	20	700	5	0.08	large hysteresis large dark current
	25	20	700	50	0.04	large hysteresis large dark current
Rutile single crystal	0	20	700	--	0.11	no hysteresis small dark current

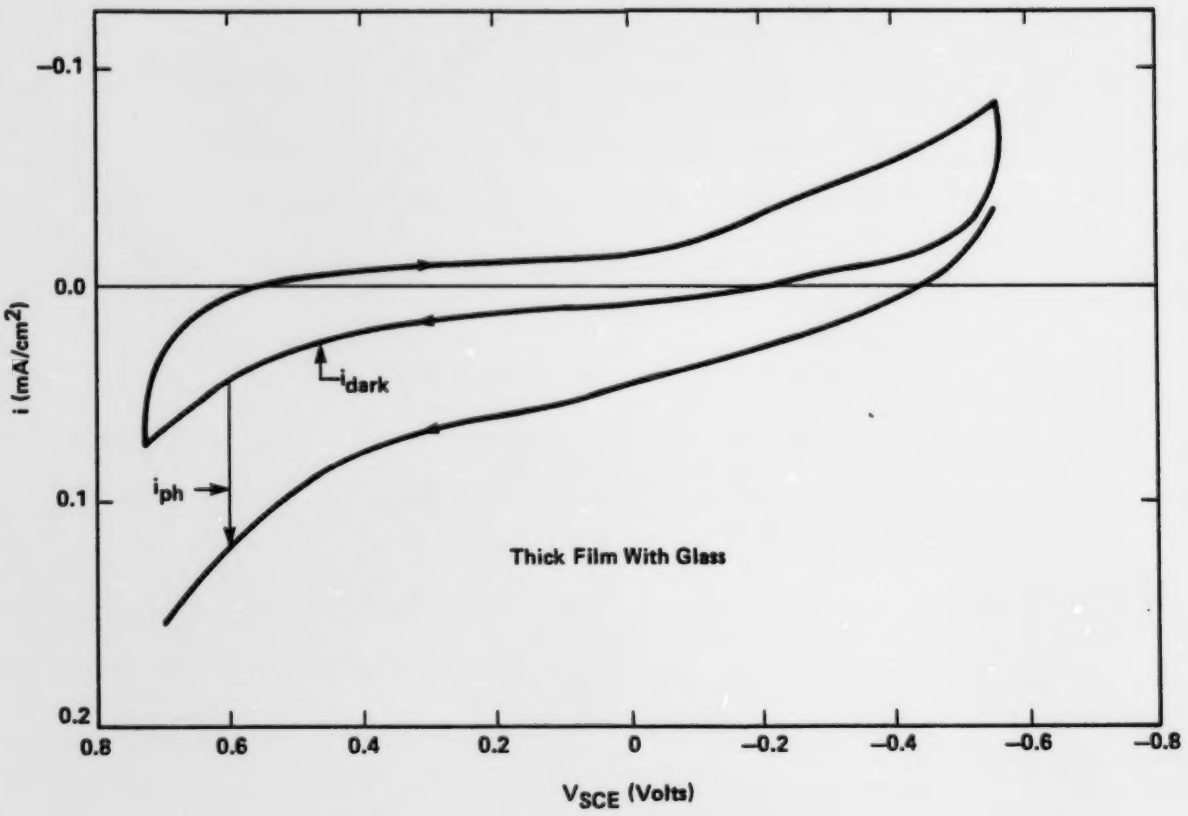

Fig. (13) Typical i-v plots for an anatase-based thick film photoanode containing 15% glass, fired at 850°C and reduced for 20 hr in NH_3.

indicated a short circuit in the film and suggested the presence of pinholes extending through the film. The use of films consisting of two layers eliminated this problem. However, further increase in the number of printed layers increased both dark current and hysteresis. The use of two layers is, therefore, considered to be optimum.

The poor PEC characteristics of the thick films observed in these preliminary experiments were attributed to at least one of the following reasons:

1. The presence of the glass binder in the film decreased both the surface area available for oxygen evolution and the volume of TiO_2 which could contribute to the photoconversion process. Also, the glass component increased the electrical resistance and thereby reduced the charge transfer processes in the film.

2. The formation of soluble forms of titanates on the film surfaces which could undergo electro-chemical reactions and cause large dark current and hysteresis.

3. The thermal reduction cycle in NH_3 induced a high concentration of O_2 vacancies in the films which can serve as traps or recombination centers (31). Also, excessive reduction may ultimately cause a phase transition to lower oxides or the formation of new compounds of poor PEC

characteristics.

IV.3 Conclusions

The conclusions drawn from this early investigation can be summarized as follows:

1. The use of glass binder in thick film TiO_2 photoanodes is undesirable. Good film adhesion can be obtained by using fritless anatase based films with particle size of $< 40\ \mu m$ and making use of the enhancement of the sintering process due to the anatase-rutile phase transformation during firing of these films at temperatures $>700\ ^\circ C$.

2. Detailed investigations on the effect of firing and thermal reduction conditions on the properties of TiO_2 films are required to understand and interpret the PEC characteristics of these films.

V. FRITLESS ANATASE - BASED THICK FILMS

V.1 Objectives and Experimental Details

Based on the preliminary results discussed in the previous section, a second series of experiments was designed to investigate the properties of fritless anatase based films and determine their optimum thermal reduction conditions for efficient PEC performance. The photoanodes used in this investigation were fabricated from two layers of anatase-based thick film separately printed and fired on Au-metallized substrates following the procedure described in Sec. III.2. The peak firing temperature was established at 900°C to provide adequate adhesion to the substrate and to be compatible with the firing temperature of the thick film Au-metallization. The samples were thermally reduced for one hour in a tube furnace using NH_3 or a mixture of Ar-20% H_2 at temperatures in the range 400-900°C. A few experiments were also carried out in a H_2 atmosphere using the belt conveyor furnace in a 30 min cycle at peak reducing temperatures in the range 500-900°C.

V.2 Results and Analysis

V.2.1 Characteristics of As-Fired Films

The thickness of the as-fired TiO_2 films was determined by a surface profilometer and optical measurements to be 30 μm. The density of the film was determined to be

approximately $2g/cm^3$. This was done by scraping the film from a measured area of the substrate and determining the weight of the powder removed. The accuracy of these measurements is estimated to be within ± 20%. For bulk TiO_2 densities are in the order of $5g/cm^3$.

X-ray diffraction and SEM analysis of as-fired photoanodes revealed a significant difference in the structure and morphology between those portions of the TiO_2 layer printed directly on the alumina substrate and those printed on the Au-metallization layer. In Fig. 14, these different portions of the film are labelled A and B, respectively. Typical x-ray spectra of these areas shown in Fig. 15 indicate that the degree of anatase-rutile phase transformation which took place during firing, is ~ 20% in area A and 80% in area B. Also, SEM micrographs (Fig. 16) show that films in area A consist of spherical particles with diameter about 0.1 - 0.2 μm while films in area B are columnar crystallites 0.5 - 1.0 μm in length and 0.1 - 0.2 μm in width.

The enhancement of phase transformation and grain growth of films printed on the gold metallization layer (area B) has been attributed to the diffusion of Au and impurities to the TiO_2 film during firing. Analysis of Du Pont 9791 thick film Au conductor has shown the presence of Cu, Cd and Pd in the range of 0.1 - 1.0% (32). PIXE

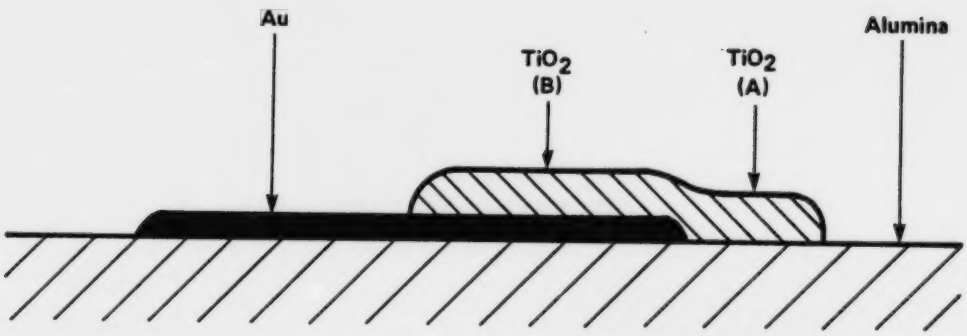

Fig. (14) A schematic diagram of a TiO_2 thick film photoanode indicating areas printed directly on the alumina substrate (A) and areas overlapped on the Au-metallization (B).

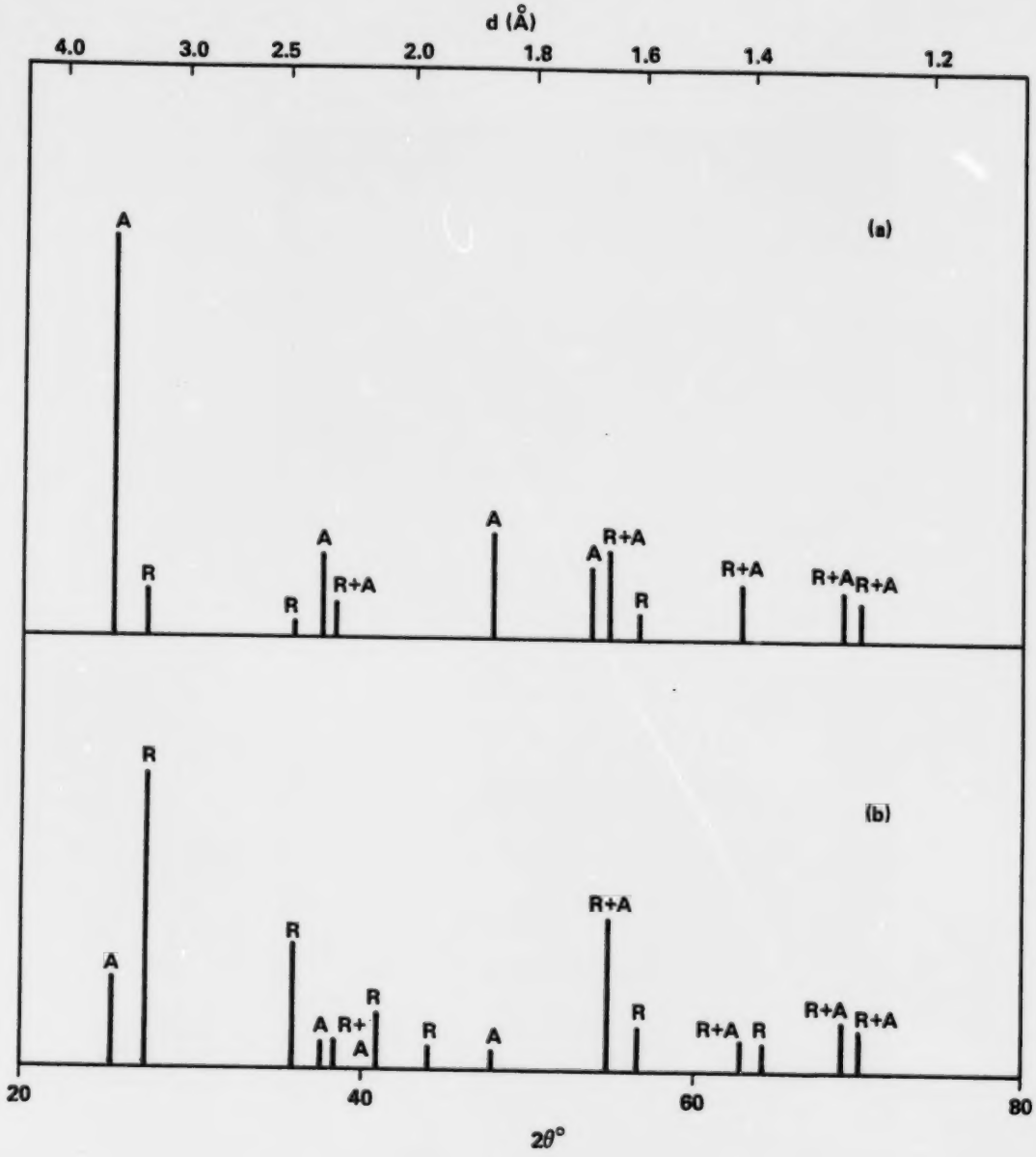

Fig. (15) X-ray spectra of anatase-based thick films as obtained from a) area (A) in Fig. 14, b) area (B) in Fig. 14. A and R refer to anatase and rutile, respectively.

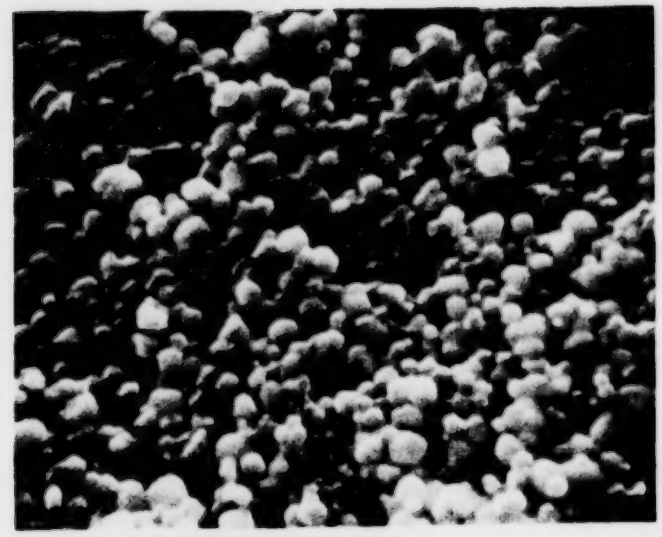

(a)

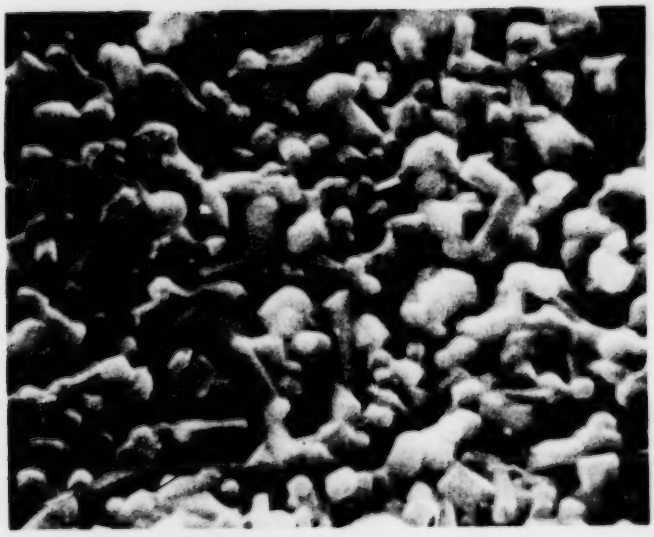

(b)

Figure 16. SEM micrograph of anatase-based thick film fired at 900°C. (a) area A of figure 14 (b) area B of figure 14.

analysis of TiO_2 films printed on Au-metallized layers showed Au and Cu which was absent from films printed directly on the alumina substrate. However, calculations showed that the depth analysis of PIXE is extended through the TiO_2 film to the Au metallization layer. Further analysis undertaken using energy dispersive x-ray analysis in the SEM has revealed Au signals in the spectra as shown in Fig. 17. Since this type of analysis is confined to ~ 1 μm in the film, the results indicated diffusion of Au into the TiO_2 films. Certain impurities are known to enhance the anatase-rutile phase transformation rate (28,33). For example, the addition of only 1% CuO would enhance the transformation rate significantly in comparison to pure films (28), as shown in Fig. 18. We believe, therefore, that the diffusion of impurities from the Au metallization to the TiO_2 film during the firing process is the primary cause of the enhanced phase transformation and grain growth in these films.

V.2.2 Characterization of reduced photoanodes

a) X-ray Analysis

TiO_2 photoanodes isochronally reduced in NH_3 showed a decrease in their x-ray diffraction line intensities with increasing thermal reduction temperatures, as shown in Fig. 19. In addition, during reduction at temperatures higher than 600°C the material gradually transformed to the TiO

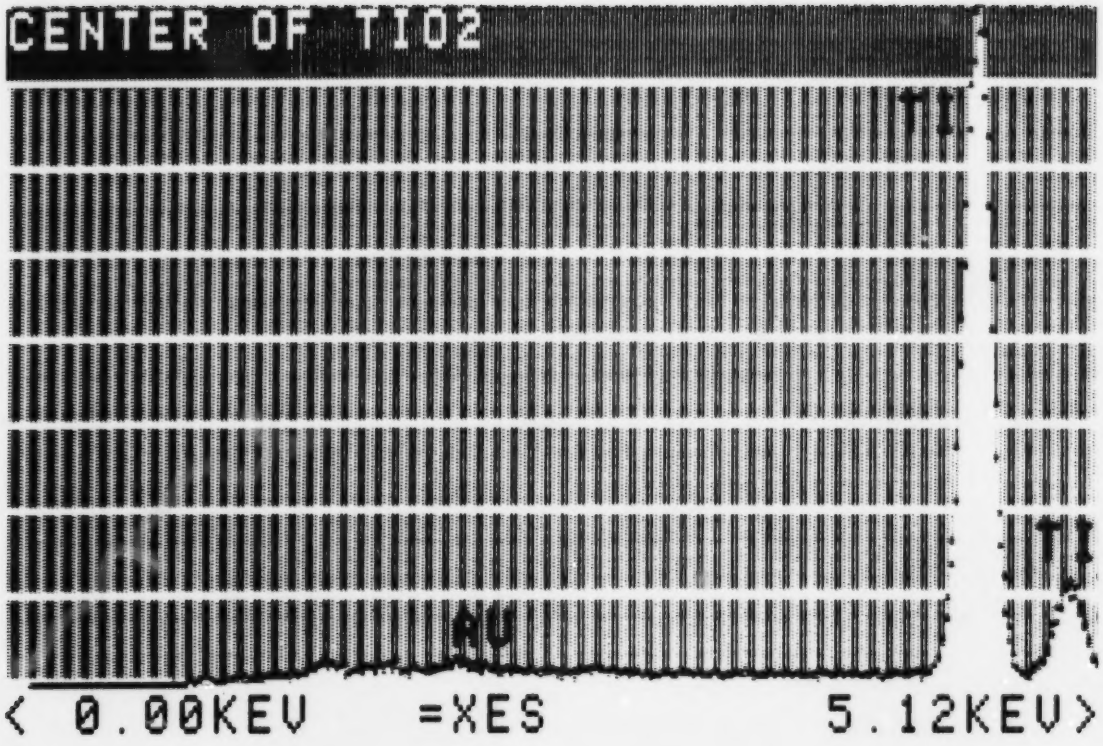

Fig. (17) An energy dispersive x-ray spectrum of anatase-based thick film obtained from area (B) (Fig. 14) of the photoanode.

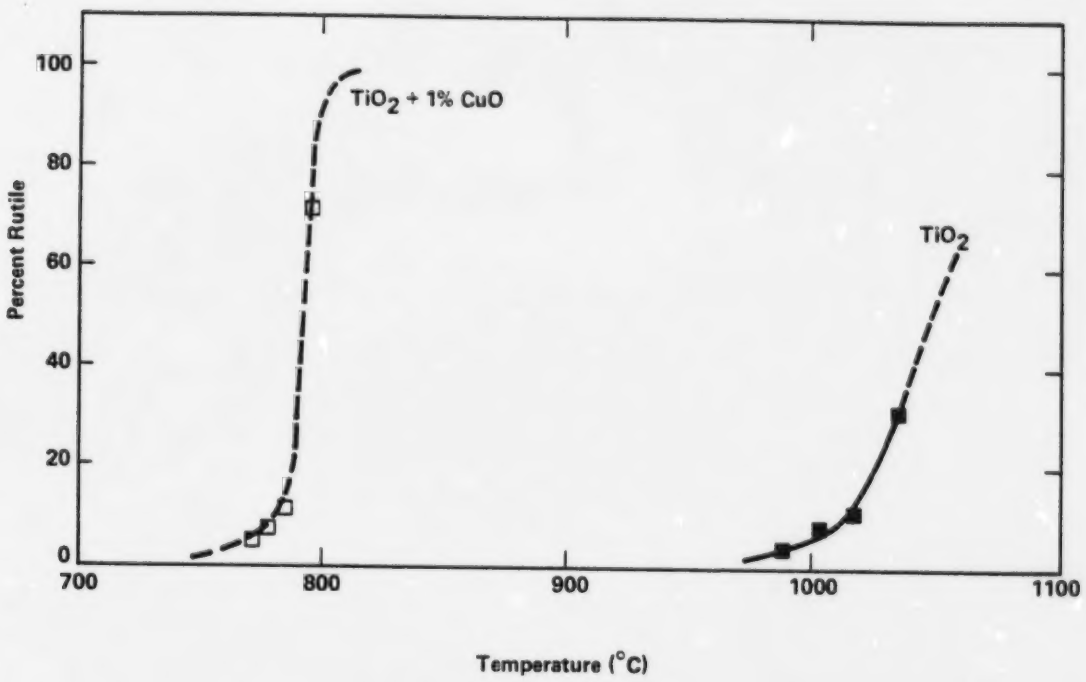

Fig. (18) The effect of 1% of CuO on the rate of anatase-rutile phase transformation (Ref. 28).

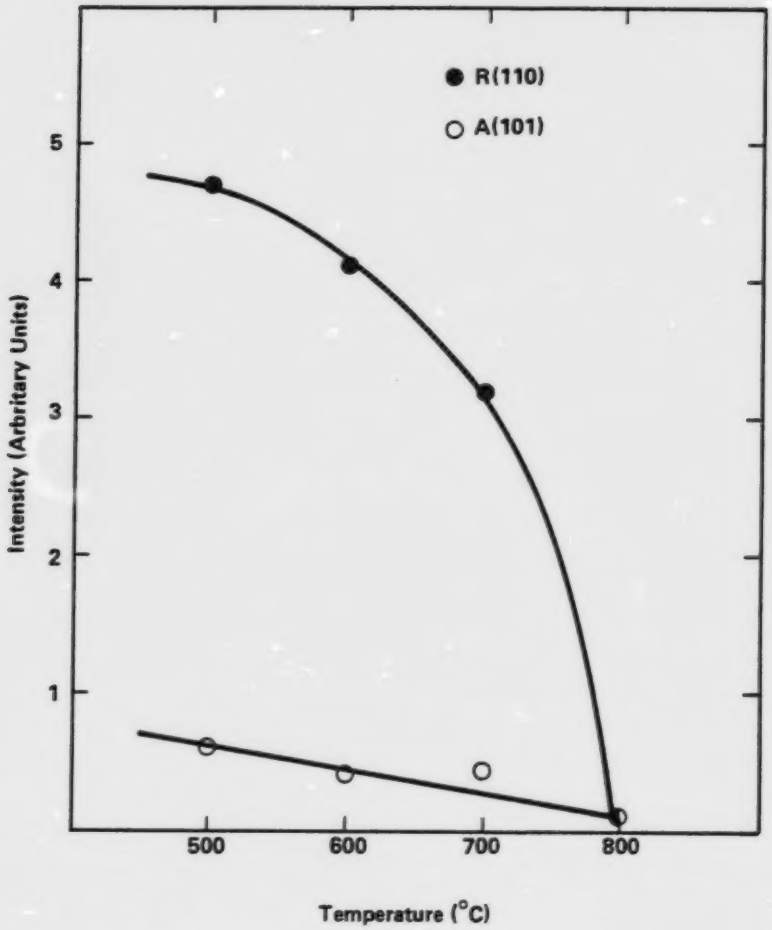

Fig. (19) Intensity of the rutile (110) and anatase (101) X-ray reflections in anodes of thick film TiO_2 reduced in NH_3 at various temperatures.

structure. This transformation was complete at 900°C with the x-ray spectra consisting of four broad peaks. As shown in Fig. 20, these can be tentatively identified as originating from the most intense peaks of the TiO structure.

A decrease in the x-ray line intensity was also observed for samples reduced in an $Ar-H_2$ gas mixture. Typical results are shown in Fig. 21. Following reduction at 900°C, all lines associated with the TiO_2 phase had disappeared and were replaced by low intensity lines located close to those of the rutile spectra. In an attempt to identify these new spectra, samples were prepared from anatase based thick films which were converted entirely to the rutile phase by a 40 hr annealing cycle in air at 900°C. These samples were then isochronally reduced for one hour in the $Ar-H_2$ gas mixture at various temperatures. New spectral components associated with the rutile peaks were first observed in samples reduced at 750°C. The number and relative intensities of these lines increased with increasing reduction temperatures as shown in Fig. 22 for x-ray diffraction spectra centered around the (110) line. This behaviour is in excellent agreement with the x-ray results reported by Anderson et al. (34) and indicated that our anodes were reduced at 900°C from TiO_2 to TiO_{2-x} where $0 < x < 0.1$. The presence of these defect structures in anatase-based films reduced in H_2 at 900°C would therefore

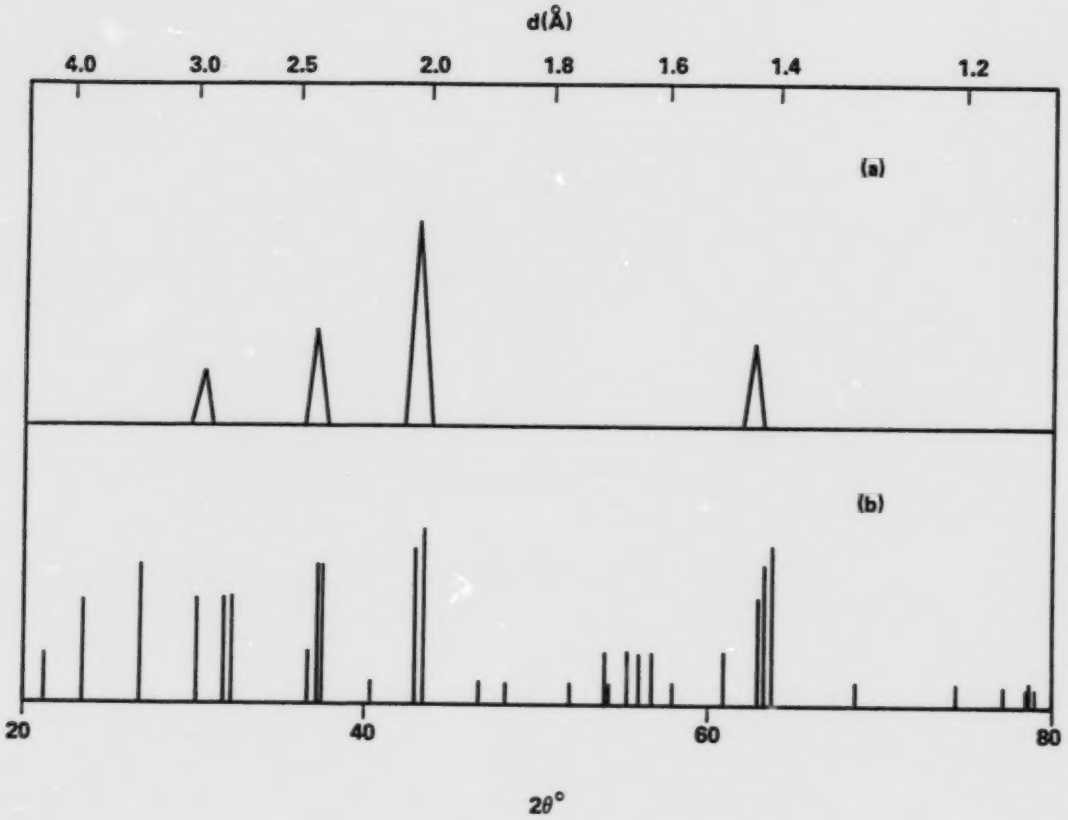

Fig. (20) (a) X-ray spectrum of anatase-based thick film reduced in NH_3 for one hour at 900°C (b) standard ASTM x-ray spectrum of the TiO structure.

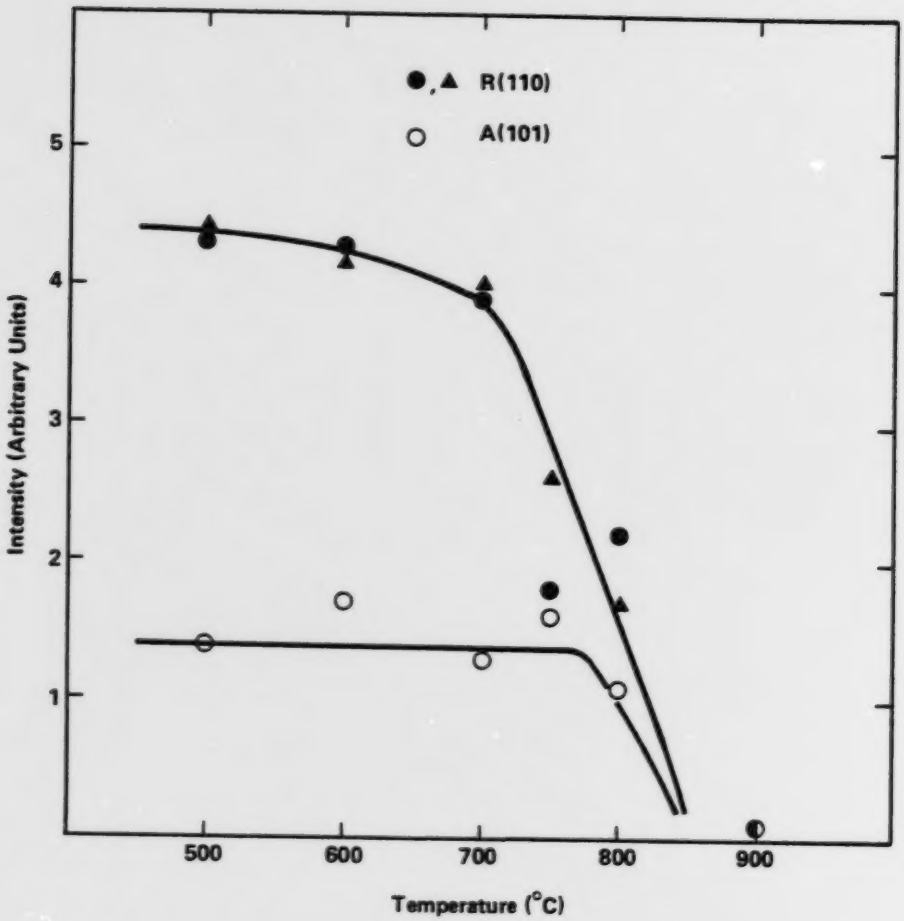

Fig. (21) Intensity of the rutile (110) and anatase (101) x-ray reflections in anatase-based thick film anodes reduced isochronally in an Ar-20% H_2 mixture. ●,○ anodes fired 15 minutes at 900°C peak temperature in air. ▲ anodes annealed 40 hrs at 900°C in air. The intensities were normalised with respect to the rutile reflection of the as-fired anode.

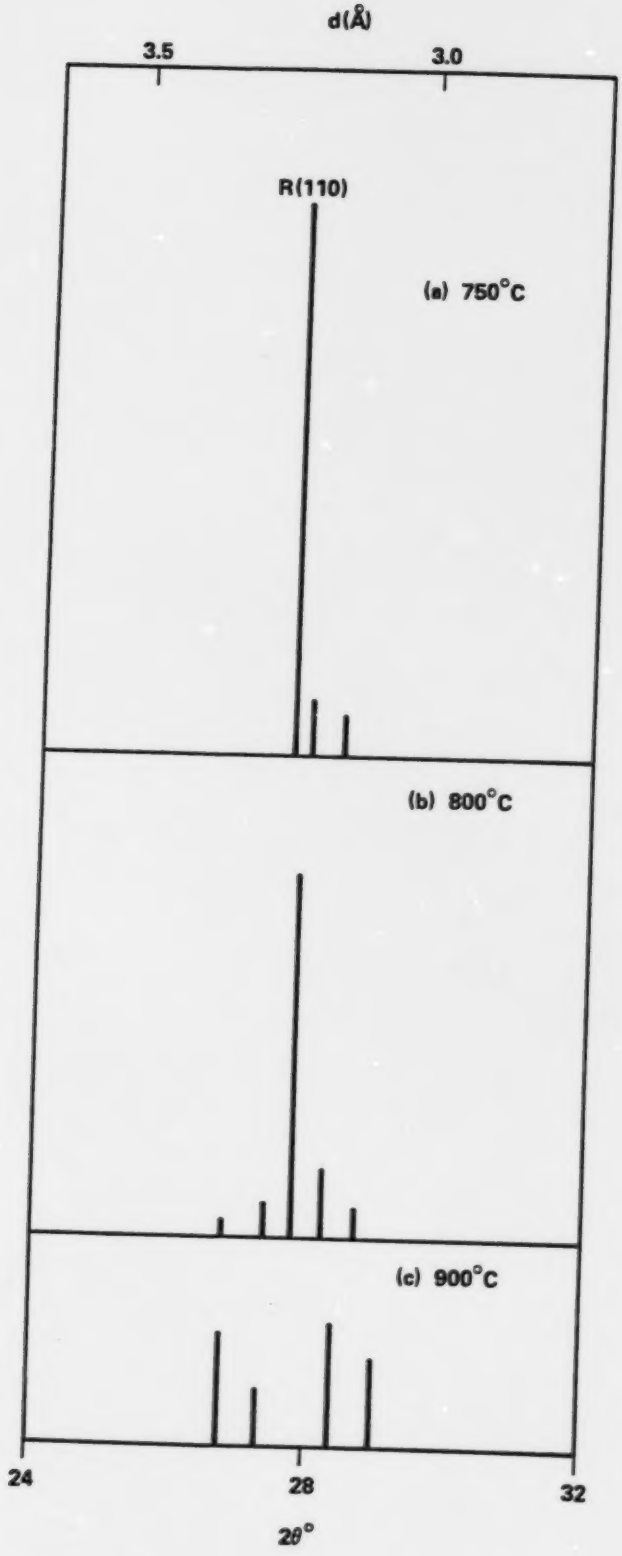

Fig. (22) X-ray reflections of anatase-based thick film reduced in Ar-20% H_2 at various temperatures.

result in the large number of low intensity spectral lines observed in these films.

b) Ion Beam Analyses

Quantative analyses of oxygen and nitrogen concentrations in reduced samples were conducted using deuteron-induced nuclear microanalysis techniques (cf. Sec. III.3.3). Fig 23 shows the results for films reduced in NH_3 and H_2 atmospheres at various temperatures. In agreement with x-ray analysis, the oxygen content in NH_3-reduced samples decreased at higher reducing temperatures as the film gradually transformed to the TiO structure. Meanwhile, a significant amount of nitrogen is incorporated in these films. X-ray analysis, however, did not reveal the formation of nitrogen-based compounds in NH_3-reduced samples. This suggested that nitrogen was not substituted in the TiO_2 crystalline lattice and may have been segregated at grain boundaries.

Films reduced in a H_2 atmosphere showed a slight reduction in oxygen content, as shown in Fig. 23. This is also in agreement with the results of the x-ray analysis indicating the formation of TiO_{2-x} phases at higher reduction temperatures.

The hydrogen content in reduced samples was determined

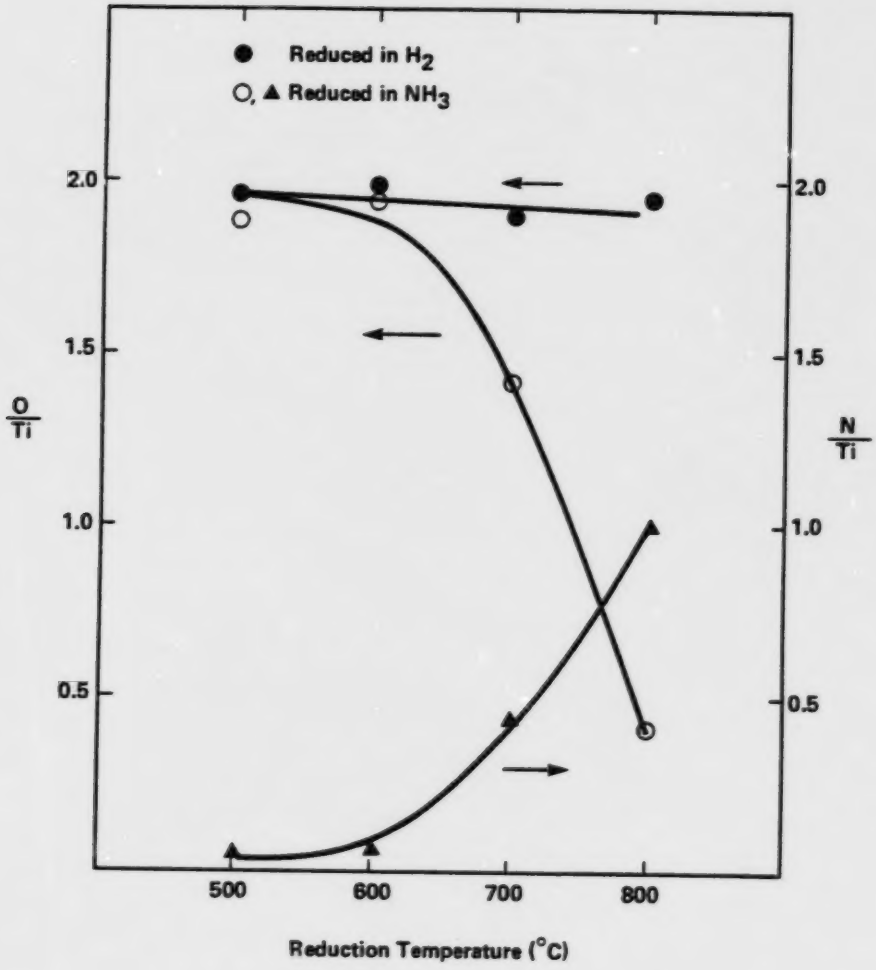

Fig. (23) The effect of one hour reduction in NH_3 and H_2 atmospheres on the oxygen and nitrogen content of anatase-based thick film anodes.

using the Elastic Recoil Detection (ERD) technique (cf. Sec. III.3.3). A typical ERD spectrum is shown in Fig. 24. The energy range of recoil events analyzed corresponds to a hydrogen depth profile of ~0.25 μm. Within this depth, the spectrum showed no significant gradient in hydrogen concentration. Results obained for films reduced in NH_3 and H_2 atmospheres at various temperatures are shown in Fig. 25. Within an estimated experimental error of ~2ppm, the amount of H_2 incorporated in the TiO_2 film is independent of the thermal reduction conditions. However, the trend towards higher concentration of H_2 in films reduced in NH_3 at 900°C may be related to the dominant TiO structure of these films.

c) SEM Analysis

The effect of reduction conditions on the morphology and grain structure of TiO_2 films is shown in Fig. 26. No changes are observed following reduction at temperatures up to 700°C in NH_3 or an Ar-H_2 gas mixture. At higher temperatures, the NH_3-reduced samples exhibited ill-defined grain morphology with diffused boundaries. However, in hydrogen-reduced samples, additional grain growth is observed.

Anatase-based films entirely converted to the rutile structure by a 40 hr annealing cycle at 900°C had large

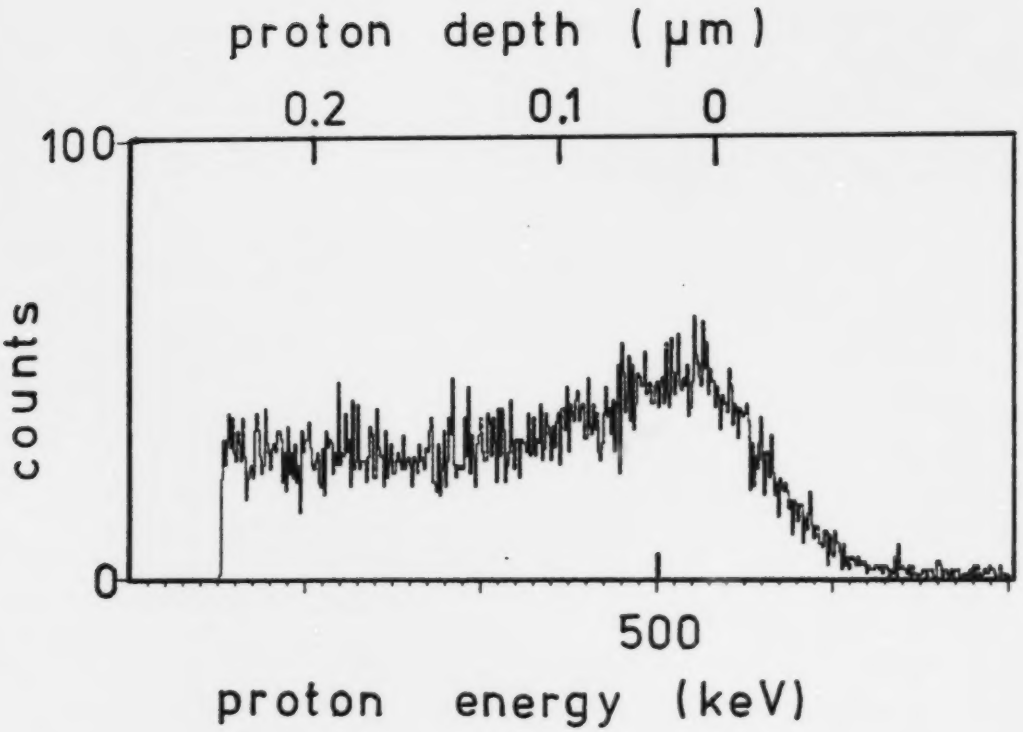

Fig. (24) ERD spectrum of an anatase-based thick film photoanode.

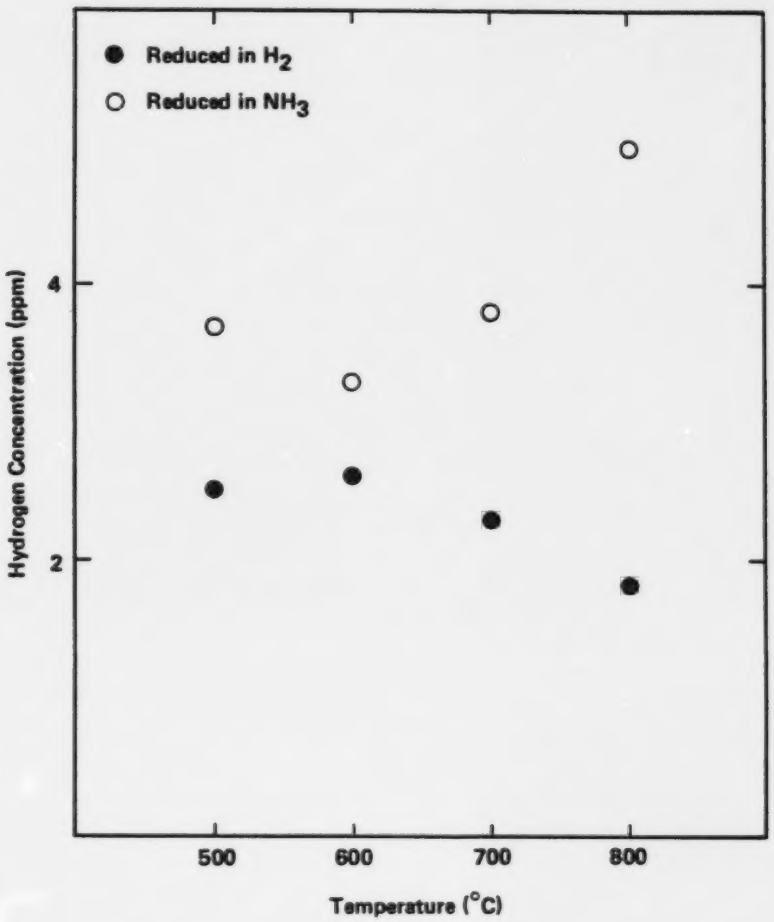

Fig. (25) Hydrogen concentration in anatase-based thick film photoanodes following reduction at various temperatures.

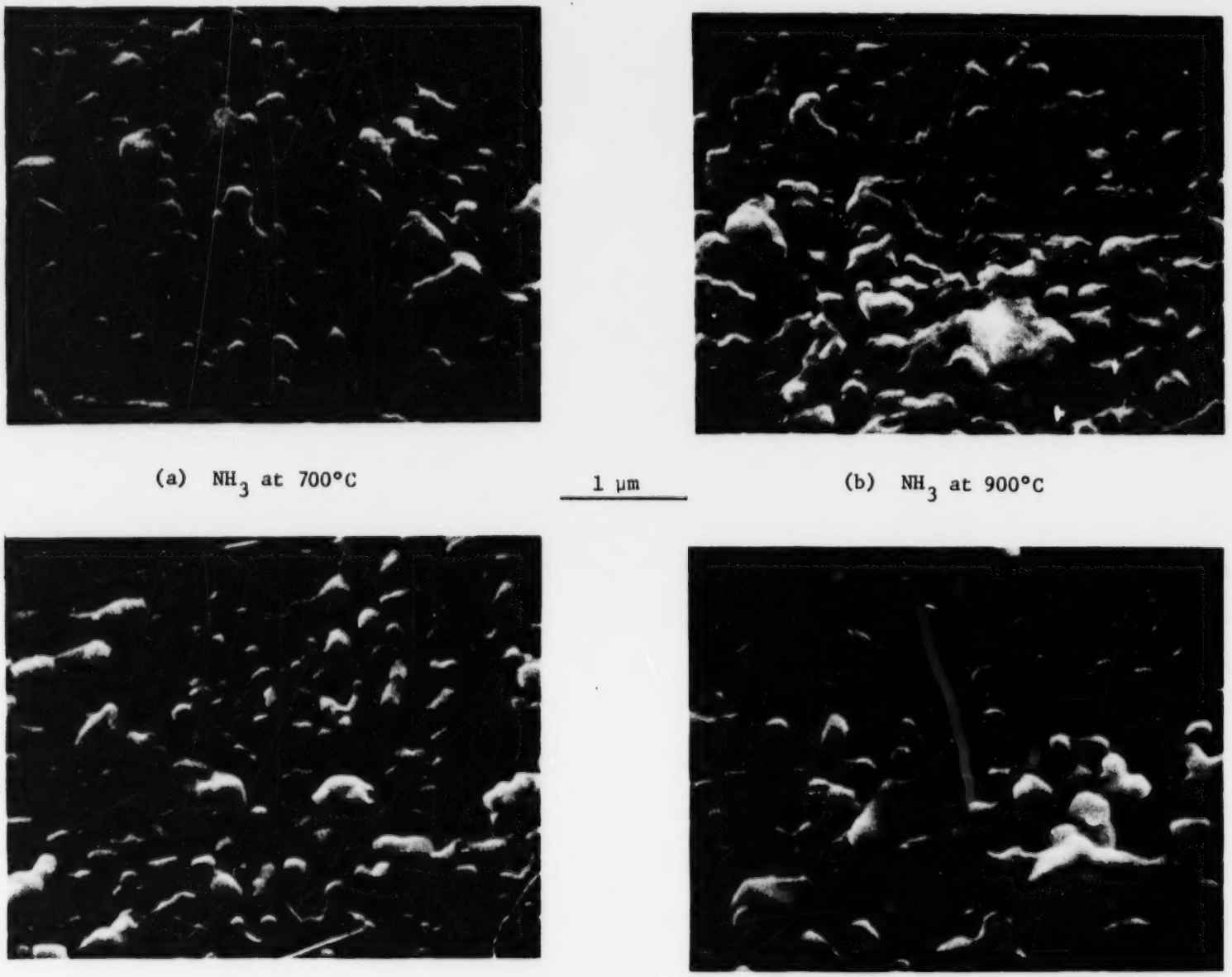

Figure 26. SEM micrographs of TiO_2 photoanodes isochronally reduced for one hour in NH_3 and H_2 atmospheres at 700°C and 900°C. The micrographs were obtained from area (B) in fig. 14.

grains with well defined crystallographic boundaries as shown in Fig. 27. No changes were observed in the morphology of these samples following their reduction in an $Ar-H_2$ gas mixture at various temperatures.

d) Resistance Measurements

The I-V characteristics of TiO_2 photoanodes were determined over several decades of applied voltage. Typical results are shown in Fig. 28. It can be seen that the resistance is constant and independent of the polarity which indicates an ohmic contact between the TiO_2 layer and the Au-metallization.

The effect of thermal reduction conditions on the anode resistance is shown in Fig. 29. Films reduced in an $Ar-H_2$ mixture undergo a gradual decline in resistance at higher reduction temperatures as the stoichiometry of the films changes from TiO_2 to TiO_{2-x}. This is compared to a sharp decrease of resistance in NH_3-reduced samples as the films rapidly transform to the metallic TiO structure. The minimum resistance of 1 Ω obtained in this case at 900°C corresponds to a bulk resistivity of 10 Ω.cm. This is much higher than the reported values for TiO of ~ 10^{-4} Ω.cm (35). Factors affecting our results include a non-uniform depth profile of resistance due to the presence of higher oxides, the low density structure of the film and the existance of

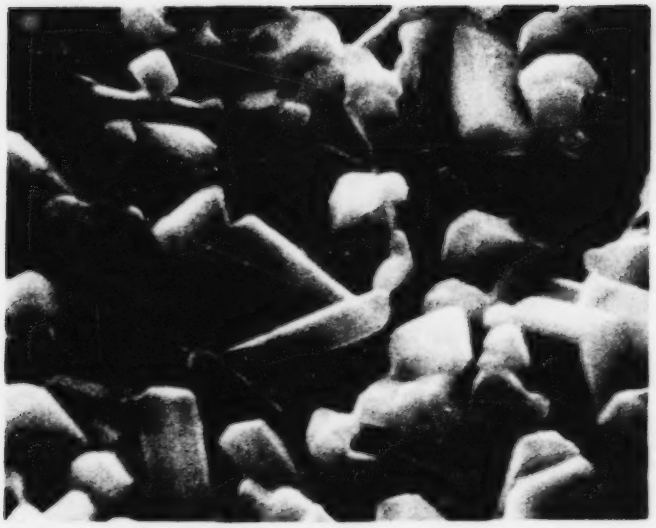

Figure 27. SEM micrograph of anatase-based film after 40 hours annealing in air at 900°C. After this annealing treatment areas A and B of figure 14 appeared identical.

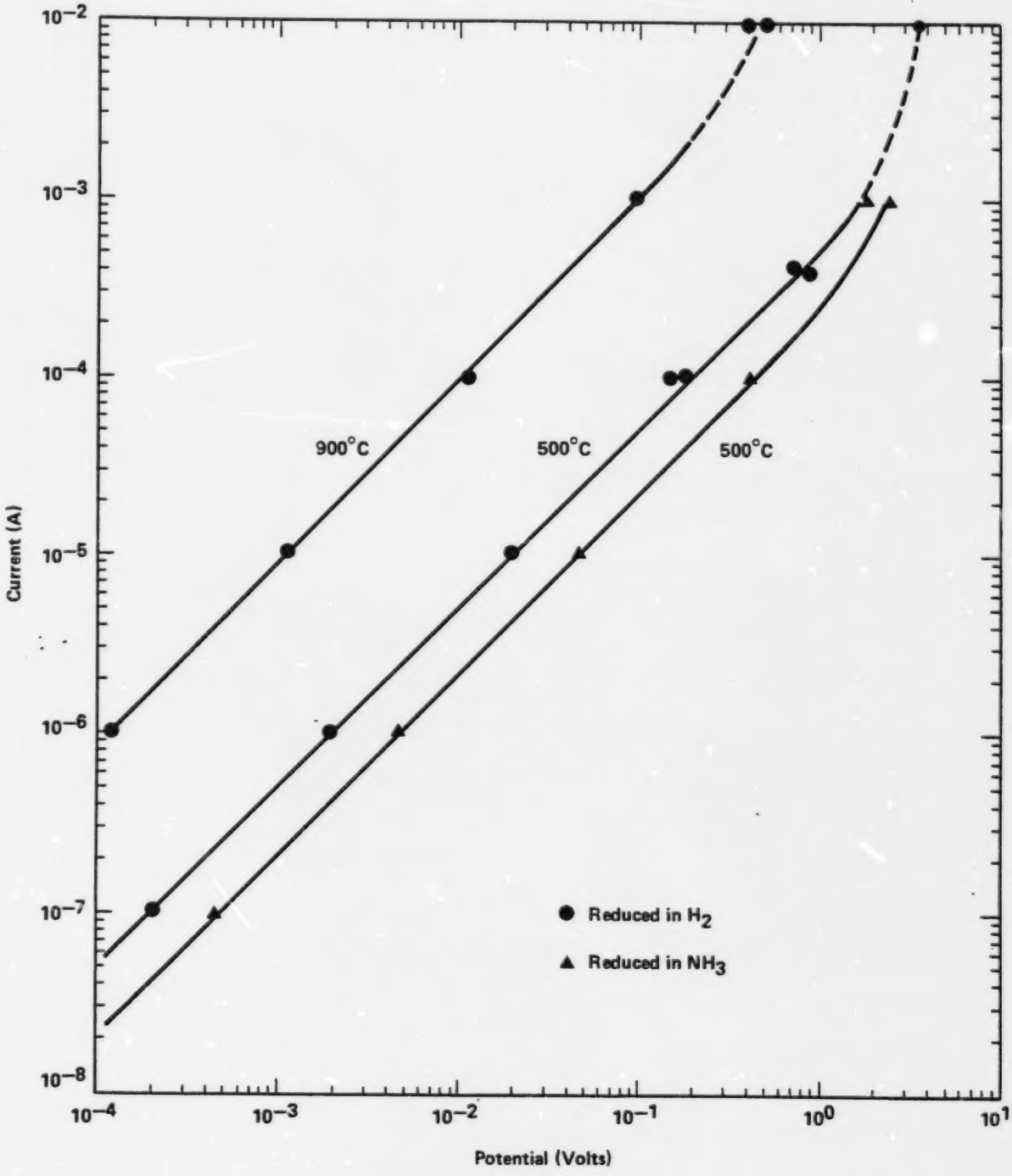

Fig. (28) I-V characteristics of anatase-based thick film photoanodes reduced at various temperatures.

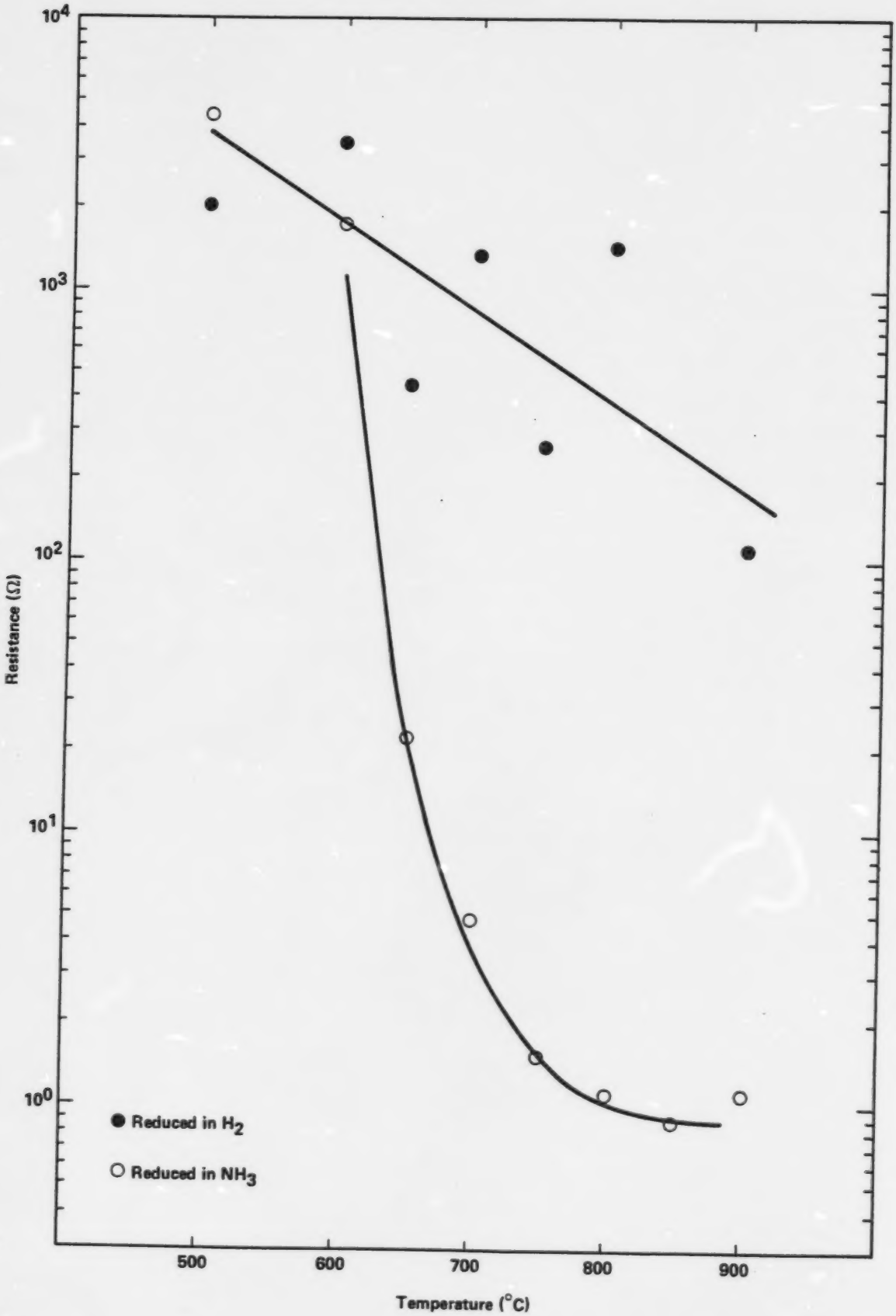

Fig. (29) Resistance of anatase-based thick film photoanodes reduced at various temperatures.

voids and microcracks. All these factors would result in high resistance values compared to those reported previously for TiO films.

e) Photoelectrochemical Measurements

Photoelectrochemical characteristics of anodes reduced in NH_3 and in an Ar-H_2 mixture were determined. Also, measurements were made on photoanodes reduced in hydrogen in a belt conveyor furnace.

In general, hydrogen reduced anodes gave stable films with low dark currents and small hysteresis in I-V plots. Typical i-v curves of an anatase-based thick film anode and a rutile single crystal are shown in Fig. 30. Photocurrents obtained under various reduction conditions for the thick film anodes are presented in Fig. 31. As shown in this figure, anodes reduced in an Ar-H_2 mixture in a tube furnace and in H_2 in a belt conveyor furnace give photocurrents of several mA/cm^2 over a range of reduction temperatures. For reduction in NH_3 , a comparable result is obtained at 500°C but at higher reduction temperatures photocurrents are much smaller.

The spectral photoresponse of a thick film TiO_2 photoanode and a single crystal of rutile, both reduced in hydrogen, are shown in Fig. 32. The spectra were

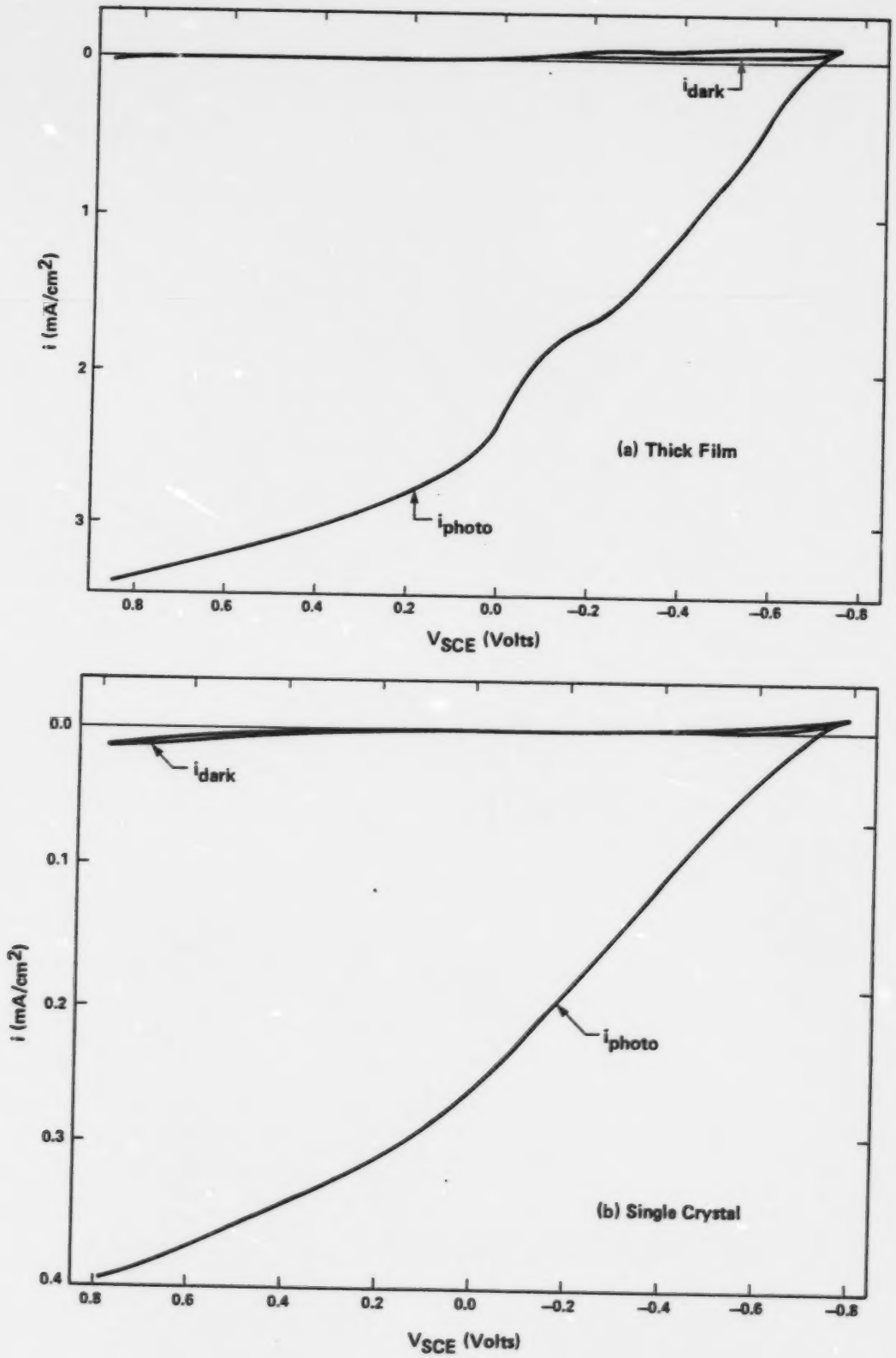

Fig. (30) i-v plots of (a) an anatase-based thick film (b) a rutile single crystal, both reduced in H_2 at 700°C. Note the difference between the two vertical scales. The measurements were conducted following the procedure described in Sec. III.3.5.

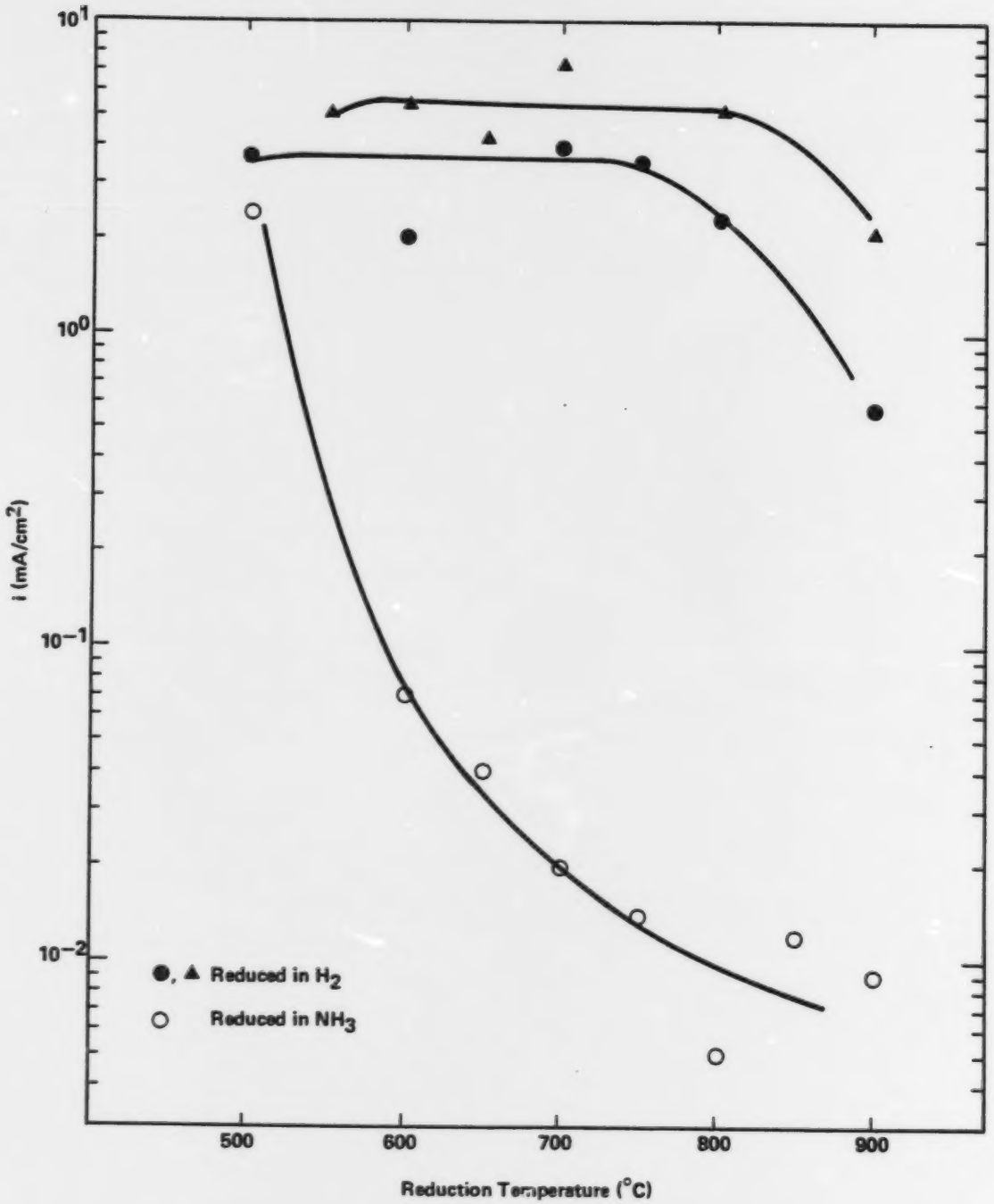

Fig. (31) Photocurrents of anatase-based thick film photoanodes, reduced at various temperatures; ●,○ in a tube furnace, ▲ in a belt conveyor furnace. The photocurrent measurements were conducted under the same conditions of solution composition, pH value, anodic bias and illumination, as described in Sec. III.3.5.

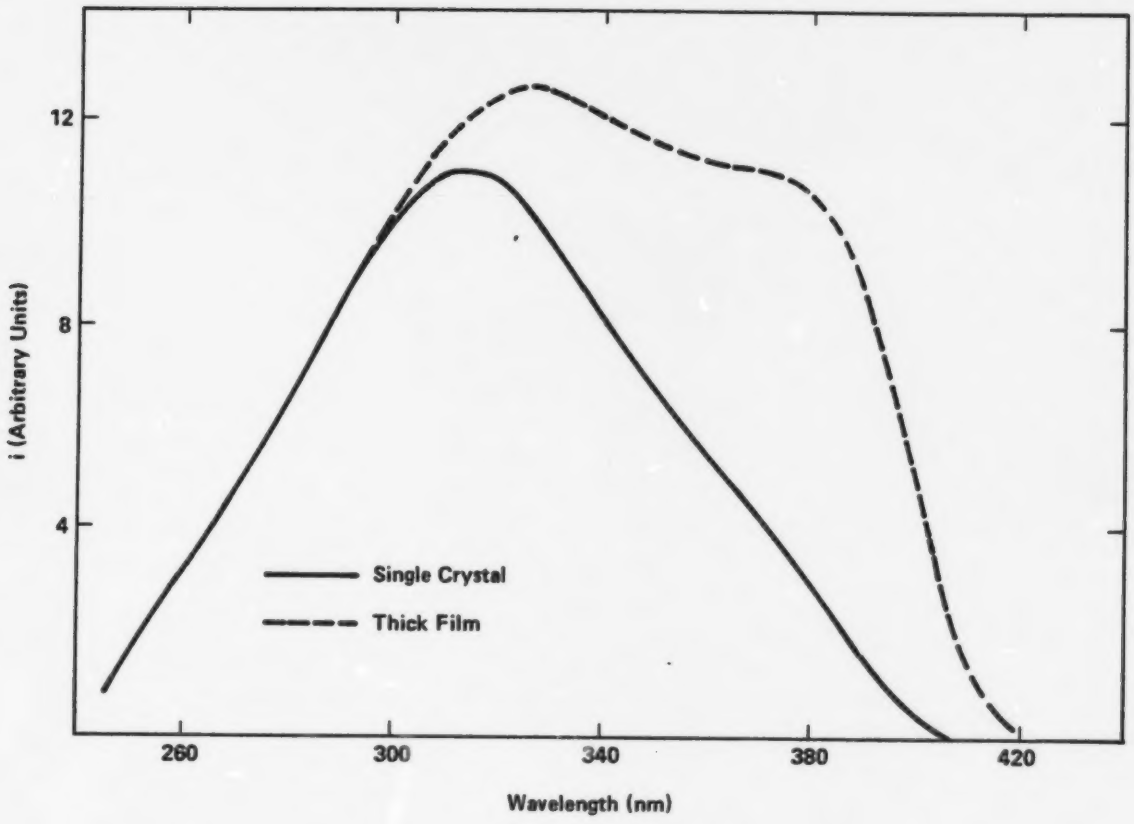

Fig. (32) Spectral photoresponse of an anatase-based thick film photoanode and a single crystal of rutile reduced in H_2. The intensity was normalised with respect to the photoresponse for wavelengths < 300 nm.

normalized with respect to the photoresponse at a wavelengths of less than 300 nm. No correction for frequency dependence of the intensity of the light source was applied. The absorption edge of the thick film photoanode has been extended toward the visible range compared to the single crystal anode, so that about 30% more energy is usefully absorbed by the film assuming the photoresponse at low wavelengths is the same for both anodes.

The solar conversion efficiency of various anodes was calculated following the procedure discussed in Sec. III.3.5. The highest efficiencies were obtained for the anatase-based films reduced in hydrogen in the belt conveyor furnace. These films yielded typical conversion efficiency of 2.5 - 3.0% with 250 mV bias. Typical values for measurements undertaken without bias were about 2.2 - 2.5%. Rutile single crystals reduced under the same conditions gave 1.5 - 1.8% efficiency, but no correction was made for IR losses.

V.3 Discussion

The results presented in this section show the significant effect of electrode preparation and properties on the PEC behaviour of fritless anatase-based thick films. The mechanisms by which each factor brings about these

effects are discussed in this section.

It seems clear that H_2-reduction of the samples at temperatures between 500 and 750°C and reduction times between 15 and 30 min produced the highest PEC performance. Studies on H_2-reduction of TiO_2 (36,37) indicated that the hydrogen molecules adsorbed on the surface and dissociated into protons which subsequently combined with the oxygen atoms in the lattice forming hydroxyl (OH^-) groups. At reduction temperatures below 750°C, the process is known to proceed without significant loss of oxygen atoms or the occurence of a major disturbance in the crystalline structure (38). This is in agreement with our x-ray and ion beam analyses. Under these conditions, the conductivity of the reduced samples may be attributed to the rupture of Ti-O-Ti bonds and the formation of $\rightarrow$Ti-O bonds and Ti^{3+} ions in the lattice. Thus, the Ti^{3+} ions act as electron donors without leaving their position in the surrounding octhedra of O atoms (39). At reduction temperatures greater than 750°C, the OH^- ions move to the surface by exchange with oxygen vacancies, forming water molecules that are finally desorbed from the surface. In this case, the conductivity is enhanced by the high concentration of oxygen vacancies at these temperatures and with the formation of disordered regions in the TiO_{2-x} lattice.

The PEC behaviour of samples reduced in hydrogen at

temperatures of less than 750 °C and durations of less than one hour are consistent with a high degree of order and low concentration of oxygen vacancies in the crystalline films. The gradual decline of photocurrents at higher reduction temperatures and longer duration can be attributed to the increasing concentration of oxygen vacancies which can serve as traps and recombination centers (31). These traps impede the separation of photogenerated electron-hole pairs and enhance their recombination.

Considerably higher reduction rates were observed in NH_3-reduced samples in comparison to H_2-reduced ones, even at relatively low temperatures. One reason for this may be a higher desorption rate of OH molecules in NH_3 gas than in H_2, thus increasing the net rate of oxygen removal from the surface of NH_3-reduced samples. This would lead to the observed high concentration of vacancies and the formation of lower oxides of metallic nature. These defects would raise the Fermi-level in NH_3-reduced samples close to the conduction band edge and reduce the band bending and field strength, that are essential for electron-hole pair separation, yielding lower photocurrents compared to H_2-reduced samples. However, other parameters may also be important such as the incorporation of high concentrations of nitrogen in NH_3-reduced films and the difference in their grain morphology compared to H_2-reduced ones.

The higher efficiency of the TiO_2 thick films is due to their large absorption of light energy, particularly in the long wavelength region ($\geq$ 300 nm), as shown in Fig. 32. This effect could be attributed to the porous structure of these films. It has been shown that the films consisted of crystals with dimensions of 0.2 - 0.5 μm, sintered together to produce an overall density less than 50% of that of bulk TiO_2. Therefore, the electrolyte is expected to penetrate deep into the bulk of the thick film. This would prevent the decrease in quantum efficiency due to recombination of photogenerated electron-hole pairs for absorption events taking place at distances from the surface layer (electric field region) larger than the minority carrier (hole) diffusion length in the film. This would, therefore, be most important in the region of long wavelength light where the absorption coefficients are low and the absorption takes place in the bulk of the film.

The impurities incorporated in the thick films, particularly transition metals and Al, could also play an important role (40-53). However, most previous studies have dealt with the effect of individual impurity elements added to pure rutile. In our case, these elements coexisted in the crystalline films and it is not possible to determine which element will be most effective in changing the PEC properties or the effects brought about by combining several dopants in the lattice.

A number of factors may also enhance the collection efficiency of photogenerated carriers in the thick films but without causing a shift in their photoresponse. These included the contact resistance at the metal/film interface, the surface conditions of the film and the presence of residual anatase phase.

In TiO_2 PEC cells, electron-hole pairs are separated by the field in the barrier region and the holes are driven to the interface with the electrolyte where they can oxidize water while the electrons are collected at the back contact and transferred to the counter-electrode where they produce hydrogen (c.f. Fig. 1). It is evident, therefore, that a high quantum efficiency is achieved if the semiconductor electrode forms an ohmic contact to the metal substrate. Although contact resistance measurements have not been undertaken, it is anticipated that the high firing temperature of the thick film and the enhancement on the anatase-rutile phase transformation at the Au-metallization interface would allow the formation of sufficiently low contact resistance. Our PEC measurements on single crystal electrodes, however, were carried out using a thin film of sputtered Au. Other workers in the field reported the use of evaporated metallic thin films, indium solder or conductive silver epoxy contacts. In these cases, no diffusion-type interface is formed and the contact

resistance is expected to be high compared to thick films.

The surface of rutile single crystal electrodes used in the present investigation was cleaned and polished. However, polishing was reported to degrade the performance of these electrodes (42,54), possibly because of the formation of surface defects which enhance the carrier combination rate in the barrier region. In the case of thick film electrodes, the topographic nature of the polycrystalline film increases the active surface area at the electrolyte interface by several orders of magnitude and increases the absorption, thereby providing higher efficiency compared to single crystal electrodes.

The improved efficiency of the screen printed films may also be related to the presence of ~20% of the anatase phase in these films. Since the results indicated an enhancement of the anatase-rutile phase transformation at the Au-metallization interface, the residual anatase structure is expected to be dominant at the surface region of the films. This is the most critical region for the charge transfer and electron transfer processes and would have a major influence on the PEC behaviour of the electrodes. However, further studies are needed before a definite conclusion can be reached regarding the role of anatase in thick film photoanodes.

V.4 Conclusions

1. Anatase-based thick films undergo a transformation to the rutile phase during the firing cycle. The diffusion of Au and impurities from the metallization layer enhances the rate of this transformation and produces films with 80% rutile compared to 20% rutile in films printed directly on the alumina substrate.

2. The PEC behaviour of anatase-based thick film anodes is quite sensitive to the reduction conditions. Insufficient reduction leads to high resistivity, large IR losses and a wide depletion region. Excessive reduction results in a high concentration of oxygen vacancies and the formation of lower oxides with metallic characteristics. These defects impede the separation of photogenerated electron-hole pairs and enhance their recombination.

3. Anatase-based films reduced in hydrogen at 700°C in a belt conveyor furnace for 30 min yielded solar energy conversion efficiencies of 2.5 - 3.0% with external bias of 240 mV and 2.2 - 2.5% without bias in 1M NaOH electrolyte at pH = 13. This is ~ 40% higher than the corresponding efficiency obtained from single crystal electrodes reduced under the same conditions. In addition, the H_2-reduced samples exhibited larger absorption of light energy in the long wavelength region.

4. The improved PEC characteristics of the screen printed thick fims have been attributed to a number of factors. These include the nature of the internal (porous) structure of the thick films, the existence of a high level of certain beneficial impurities, low contact resistance at the back metallization interface, high absorption surface with large semiconductor/electrolyte interface, and the presence of a residual anatase layer at the film surface. However, it has not been possible to determine the relative importance of each of these parameters on the PEC behaviour of TiO_2 thick film photoanodes.

VI. COMPLEMENTARY INVESTIGATIONS

VI.1 Objectives

In the previous section, the presence of residual anatase and the incorporation of impurities in anatase-based thick film were considered among the important parameters which cause the high PEC performance of these films compared to single crystal rutile. In this section, we present results of preliminary investigations undertaken to provide more insight into the effects of these parameters.

VI.2 The Effect of The Anatase Phase

The effect of the anatase structure was investigated using pastes containing various mixtures of rutile and anatase powders. The percentage of rutile in these pastes varied between 50 and 90%. After firing in a belt conveyor furnace at 900°C, the percentage of rutile phase in the films printed on Au-metallized substrates was 90 - 98%. This compared to ~ 80% rutile in samples prepared from anatase powder only and subjected to the same firing cycle.

The photocurrents of the films after a 30 min H_2-reduction cycle in the belt conveyor furnace at a peak temperature of 700°C are shown in Fig. 33. No dependence on film structure is observed except for a lower value of the photocurrent in the sample of lowest initial anatase content (10%). The anatase powder was initially introduced

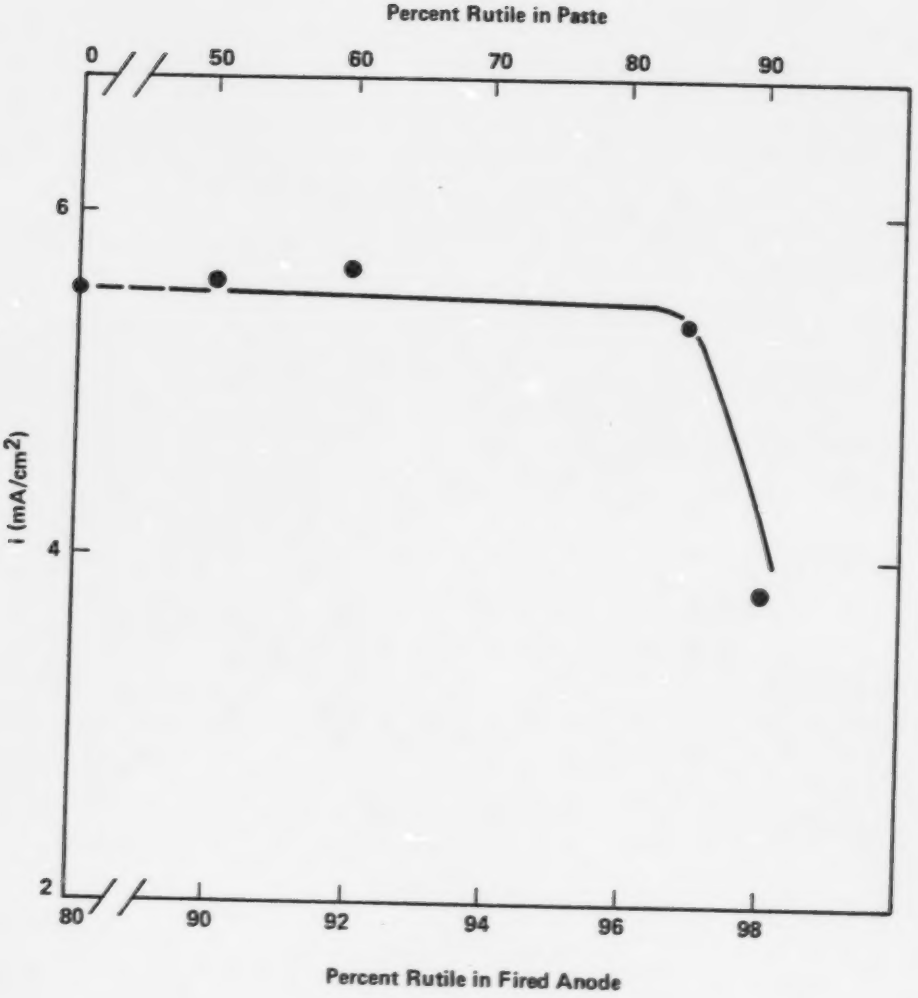

Fig. (33) Photocurrents of thick film photoanodes prepared from pastes containing various mixtures of anatase and rutile.

to promote adhesion of the thick film during the anatase-rutile phase transformation. However, the presence of at least a small percentage of the anatase phase in the film seems to be necessary for achieving acceptable PEC characteristics. This may be attributed to better adhesion in films containing anatase or most probably due to a basic difference in the photoelectrochemical properties of rutile and anatase. No definite conclusions can be reached through this preliminary investigation.

VI.3 The Effect of Dopants

The effect of dopants was investigated using pastes containing mixtures of anatase and various dopants. The dopants chosen were Al and a number of 3d transition metals. The actual chemicals used as dopants along with their suppliers are listed in table III. These materials were ground down and passed through a 400 mesh sieve. They were then added individually to anatase-based paste to provide a final composition with 5% dopants. The photoanodes were prepared by firing at 900°C in air followed by a 30 min H_2 reduction cycle in the belt conveyor furnace at a peak temperature of 700°C.

The effects of doping on the photocurrent response of the TiO_2 films are summarized in table IV. Only Al_2O_3 doped TiO_2 films were found to exhibit improved photoresponse compared to the undoped samples, in agreement with previous

TABLE III

Materials used as dopants in anatase-based thick film pastes

(only technical grade materials were used)

Material	Supplier
Al_2O_3	Philipp Brothers
V_2O_3	Baker
Cr	BNR stock
MnO_2	Baker
Fe_2O_3	JMM
Co	BNR stock
NiO	Baker
Cu_2O	Alfa

work (e.g. 40,48 and 55). It has been suggested that Al doping increases the minority carrier diffusion length, which in turn permits an increase in the collection efficiency of photogenerated carriers. In addition, Al-doping may be responsible for the stabilization of Ti^{3+} donor centers generated by thermal reduction and also for the creation of surface states which are essential for the oxidation of OH^- ions.

All other dopants caused a decrease in the photocurrent and thereby a lower conversion efficiency than undoped samples, as shown in table IV. In addition, they were found to extend the absorption spectrum of TiO_2 towards the longer wavelength side of the solar spectrum. For example, the effect of Cr-doping on the photocurrent spectrum is shown in Fig. 34. These results are also in agreement with previous reports in the literature (42,43). This behaviour was attributed to the formation of intermediate levels in the bandgap, which can originate from impurity cations and/or from defects induced by the doping. These can sustain photo-induced electron-hole generation at longer wavelengths but can also act as recombination centers.

The results shown in table IV also indicate that annealed films completely converted to rutile generally exhibited lower photocurrents than unannealed films. This emphasized once again the role which might be played by

TABLE IV

The ratio of photocurrents of doped and undoped anatase-based TiO_2 thick film photoanodes reduced for 30 min in H_2 at a peak temperature of 700°C.

Dopant	i(doped)/i(undoped)
V_2O_3	0
Cr	0.4
MnO_2	0.8
Fe_2O_3	0
Co	0
NiO	1.0
Cu_2O	0
Al_2O_3	1.5

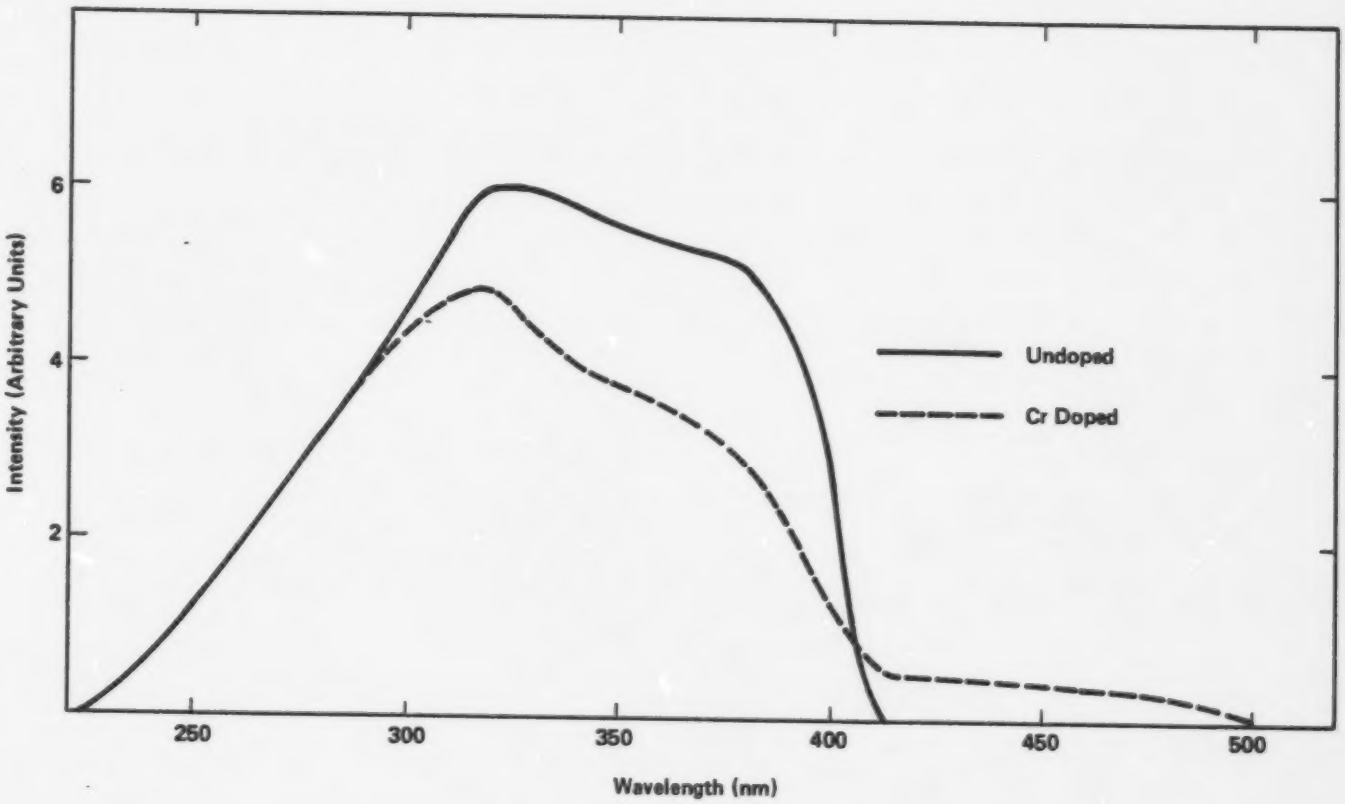

Fig. (34) Spectral photoresponse of anatase-based thick film photoanodes, prepared with and without the addition of Cr to the paste. The intensity was normalized with respect to the photoresponse for wavelengths < 300 nm.

residual anatase phase in the thick film anodes.

VI.4 Conclusions

(1) The presence of the anatase phase in TiO_2 thick film is necessary to achieve high photocurrents. However, the reason for this needs further investigation.

(2) The addition of Al_2O_3 improves the photocurrent response of anatase-based film, and thereby its solar conversion efficiency, while 3d transition metals such as Cr decrease the conversion efficiency but increase the wavelength response in the visible region.

VII OVERALL CONCLUSIONS

The feasibility of fabricating inexpensive, stable thick film screen printed TiO_2 anodes has been successfully demonstrated for the first time. The performance of these anodes in photoelectrochemical cells was found to be superior to that of anodes prepared from rutile single crystals.

For practical applications, the thick film technique offers several advantages over other fabrication techniques. Among these are the following:

1. The film composition and structure can be easily monitored, controlled and modified during various fabrication stages.

2. The films produced are mechanically durable, withstand dissolution in electrolytes and can be restored to their original forms by re-oxidation and reduction.

3. The printing process is simple and can be easily modified for application to a variety of large area, low cost substrates including ceramics, glass and porcelain steel.

4. The thick film process is ideally suited to mass

production with relatively low investment in capital equipment and personnel training.

According to the present work, the most favorable conditions for the preparation of TiO_2 thick film for efficient photoelectrolysis of water are the following:

1. The pastes should be formulated from TiO_2 powder of the anatase structure having particle size of less than 40 μm. The transformation of anatase to rutile during high temperature processes provides good adhesion of the films to the substrate without using a glass binder. In aidition, the presence of anatase phase in the TiO_2 electrodes seems to be necessary to obtain good PEC characteristics.

2. The screen printed thick film TiO_2 should be fired in a belt conveyor furnace with a 90 min cycle in air at a peak firing temperature of 900°C. This procedure allows sufficient phase transformation in the anatase-based film to provide adequate adhesion to the substrate and low contact resistance with the thick film back metallization.

3. The use of two layers of TiO_2 thick films separately printed and fired is necessary to eliminate short circuits caused by pinholes.

4. A 30 min H_2 reduction cycle in a belt conveyor furnace

at a peak temperature of 700°C produced photoanodes with maximum solar conversion efficiency. Insufficient reduction leads to high resistivity materials with large IR losses and a wide depletion region. Reduction in ammonia or excessive reduction in hydrogen produced defects which impede the separation of photogenerated electron-hole pairs and enhance their recombination.

5. The addition of Al_2O_3 to anatase-based thick films is recommended for improved PEC efficiency. The use of 3d transition metal dopants in these films reduced the overall conversion efficiency but increased the wavelength response in the visible region.

The work described in this report was planned as a first phase to establish the feasibility of fabricating TiO_2 thick film photoanodes. Although this goal has been achieved, many aspects should be considered for further investigation in subsequent stages of this program. Some of these are the following:

1. Study the kinetics of charge transfer at the polycrystalline TiO_2 thick film/electrolyte interface.

2. Establish an understanding of the influence of impurities in anatase-based thick film materials and their defect structure on the PEC properties.

3. Evaluate the reliability and aging mechanisms of TiO_2 thick film photoanodes under different PEC conditions.

4. Explore dopant species that can provide both higher conversion efficiency and a sufficient shift in the wavelength response toward the visible range.

5. Develop low cost thick film base metal contacts to replace Au metallization in TiO_2 photoanodes and investigate their contact properties.

6. Investigate the feasibility of using the thick film technique in the preparation of other materials of interest in water photoelectrolysis such as $SrTiO_3$.

The potential economic benefits of photoelectrolysis depend on the efficiencies of the photoelectrolytic process in comparison to alternative technologies. It is generally claimed that any practical "Solar Cell" must have an efficiency of at least 10% in order to cover various fabrication and installation costs. At present, there is no fundamental reason that can prevent the development of a PEC cell with the same or better efficiency as a solid state device with the same band gap. If this goal is achieved, thick film processes can certainly be a viable technique for the low cost fabrication of efficient photoelectrodes.

References

1. H.P. Maruska and A.K. Ghosh, Solar Energy, 20 (1978) 443.

2. K. Rajeshwar et al, Electrochimica Acta, 23 (1978) 1117.

3. A.J. Nozik, Proc. 2nd World Hydrogen Energy Conf., Zurich, (1978) p. 1217.

4. L.A. Harris and R.W. Wilson, Ann. Rev. Mat.Sci. 8 (1978) 99.

5. J.G. Mavroides, Mat. Res. Bull. 13 (1978) 1379.

6. M.A. Butler and D.S. Ginley, J. Mat. Sci., 15 (1980) 1.

7. J.M. Bolts and M.S. Wrighton, J. Phys. Chem. 80 (1976) 2641

8. K.L. Hardee and A.J. Bard, J.Electrochem. Soc. 122 (1975) 739.

9. K.L. Hardee and A.J. Bard, ibid, 124 (1977) 215.

10. J.G. Mavroides et al., Mat. Res. Bull 10 (1975) 1023.

11. J.F. Houlihan and D.P. Madacsi, ibid, 11 (1976) 1191.

12. J. Kennedy et al., Nature 253 (1975) 719.

13. A. Fujishima et al., J. Electrochem. Soc., 122 (1975) 1487.

14. R. Wang and C.H. Henager, ibid, 126 (1979) 83.

15. W. Gissler et al., J. Appl. Electrochem., 6 (1976) 9.

16. A.A. Soliman and H.J.J. Seguin, Solar Energy

Materials 5 (1981) 95.

17. R. Borek et al., Microelectronics & reliability 11 (1972) 511.

18. B. Licznerski and K. Nitsch, Electrocomponent Sci. & Tech 4 (1977) 1.

19. "Handbook of Thick Film Hybrid Microelectronics", C.A. Harper, Ed., McGraw-Hill, N.Y. (1974).

20. "Handbook of Thin Film Technology", L.I. Maissel, Ed., McGraw-Hill, N.Y. (1974).

21. C.M. Anderson and H.M. Naguib, Int. J. Hyb. Microelectronics 4 (1) (1981) 24.

22. R.A. Spurr and H. Myers, Annl. Chem., 29 (1957) 760.

23. P. Mazzoldi andG. Della-Mea, Thin Solid Films, 77 (1981) 181.

24. B.L. Doyle and P.S. Peercy, Appl. Phys. Lett. 34 (1979) 811.

25. D. Amm et al., J. Can. Ceram. Soc. 50 (1981) 1.

26. F. Follemann et al., Nucl. Instr. and Meth. 116 (1974) 487.

27. W. Reuter et al., J. Appl. Phys. 46 (1975) 3914.

28. R.D. Shannon and J.A. Pask, J. Am. Ceramic Soc. 48 (1965) 391.

29. J.A. Hedvall, "Reactivity of Solids", Edwards Brothers Inc., Ann Arbor, Mich. (1943) p. 127.

30. "Handbook of Materials Science", C.T. Lynch, Ed., CRC Press, Clev., Ohio, Vol. I (1974) p. 235.

31. S.N. Subbarao et al., Mat. Res. Bull., 13 (1978)

1461

32. J.P. Cummings and A.D. Beck, Proc. 1978 Int. Symp. of Hyb. Microelectronics (ISHM), p. 280.

33. K.J.D. MacKenzie, J. Brit. Ceramic Soc. 74 (1975) 29.

34. S. Anderson, Acta Chem. Scand. 11 (1957) 1641.

35. D. Adler, Solid State Physics, Ed. F. Seitn, D. Turnbull and H. Ehrenreich, 21 (1968) p. 86.

36. T. Iwaki et al., J. of Catalysis 39 (1975) 324.

37. T. Iwaki and M. Miura, Bull. Chem. Soc. Jap. 49 (1976) 2321.

38. G.J. Hill, Brit. J. Appl. Phys. (J. Phys. D) 1 (1968) 1151.

39. L.A. Harris and R. Schumacher, J. Electrochem. Soc., 127 (1980) 1186.

40. J. Augustynski et al., J. Electrochem. Soc. 124 (1977) 1063.

41. G. Blondeau et al., J. Electrochem. Soc. 126 (1979) 1592.

42. A.K. Ghosh and H.P. Maruska, J. Electrochem. Soc. 124 (1977) 1516.

43. A. Monnier and J. Augustynski, J. Electrochem. Soc. 127 (1980) 1576.

44. R.D. Rauh et al., J. Phys. Chem. 83 (1979) 2221.

45. M. Shionawa et al., Yogyo - Dyokai - Shi 83 (1975) 471.

46. C. Stalder and J. Augustynski, J. Electrochem. Soc.

126 (1979) 2007.

47. Y. Matsumato et al., J. Electrochem. Soc. 127 (1980) 2148.

48. P. Salvador, Mat. Res. Bull. 15 (1980) 1287.

49. J.F. Juliao et al., J. Electrochem. Soc. 127 (1980) 2264.

50. G. Campet et al., Mat. Res. Bull. 15 (1980) 1135.

51. K. Minushima et al., J. Phys. Soc. Japan 32 (1972) 1519.

52. K. Minushima et al., J. Phy. Chem. Solids 40 (1979) 1129.

53. M.A. Butler et al., J. Electrochem. Soc. 128 (1981) 200.

54. R.H. Wilson et al., J. Electrochem. Soc. 126 (1979) 844.

55. J.F. Houlihan et al., Mat Res. Bull., 13 (1978) 1205, and ibid 14 (1979) 915.